

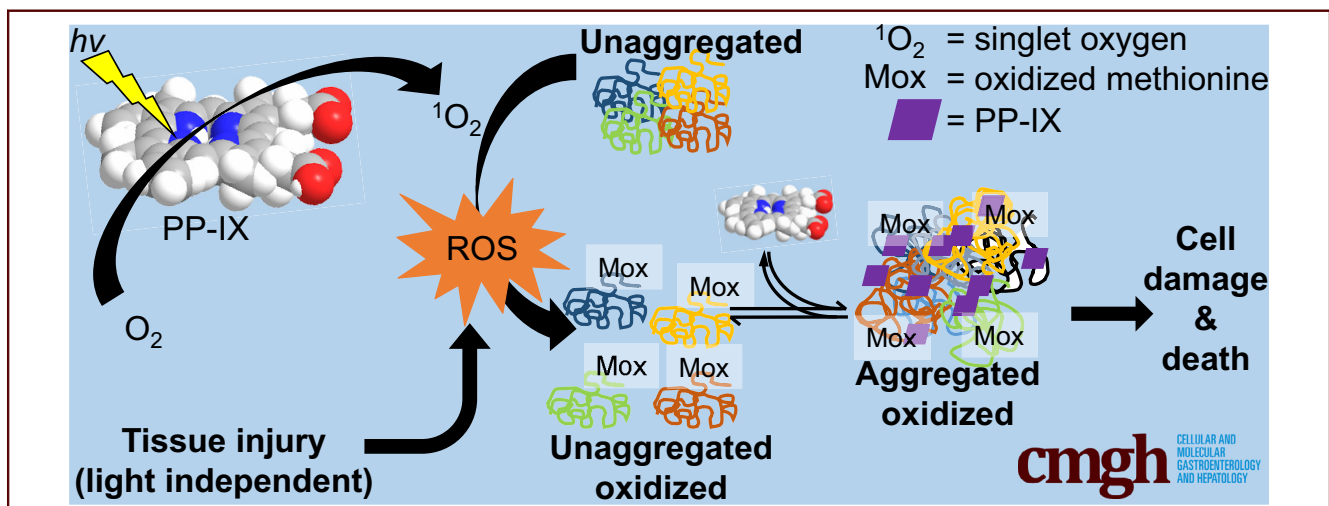
ORIGINAL RESEARCH

Oxygen and Conformation Dependent Protein Oxidation and Aggregation by Porphyrins in Hepatocytes and Light-Exposed Cells



Dhiman Maitra,¹ Eric L. Carter,² Rani Richardson,¹ Laure Rittié,³ Venkatesha Basur,⁴ Haoming Zhang,⁵ Alexey I. Nesvizhskii,⁴ Yoichi Osawa,⁵ Matthew W. Wolf,⁶ Stephen W. Ragsdale,² Nicolai Lehnert,^{6,7} Harald Herrmann,^{8,9} and M. Bishr Omary^{1,10,11}

¹Department of Molecular and Integrative Physiology, ²Department of Biological Chemistry, ³Department of Dermatology, ⁴Department of Pathology, ⁵Department of Pharmacology, ⁶Department of Chemistry, ⁷Department of Biophysics, University of Michigan, Ann Arbor, Michigan; ⁸Institute of Neuropathology, University Hospital Erlangen, Erlangen, Germany; ⁹Division of Molecular Genetics, German Cancer Research Center, Heidelberg, Germany; ¹⁰Department of Internal Medicine, University of Michigan Medical School, Ann Arbor, Michigan; ¹¹Cell Biology, Faculty of Science and Technology, Åbo Akademi University, Turku, Finland



SUMMARY

Porphyrias are genetic diseases caused by disruption of heme biosynthesis and accumulation of toxic porphyrins. Porphyrias cause liver damage, photosensitivity, and neurovisceral symptoms. We define the mechanism of porphyrin-mediated protein aggregation and its role in porphyrin-induced cell damage.

BACKGROUND & AIMS: Porphyrias are caused by porphyrin accumulation resulting from defects in the heme biosynthetic pathway that typically lead to photosensitivity and possible end-stage liver disease with an increased risk of hepatocellular carcinoma. Our aims were to study the mechanism of porphyrin-induced cell damage and protein aggregation, including liver injury, where light exposure is absent.

METHODS: Porphyria was induced in vivo in mice using 3,5-diethoxycarbonyl-1,4-dihydrocollidine or in vitro by exposing human liver Huh7 cells and keratinocytes, or their lysates, to protoporphyrin-IX, other porphyrins, or to δ -aminolevulinic

acid plus deferoxamine. The livers, cultured cells, or porphyrin exposed purified proteins were analyzed for protein aggregation and oxidation using immunoblotting, mass spectrometry, and electron paramagnetic resonance spectroscopy. Consequences on cell-cycle progression were assessed.

RESULTS: Porphyrin-mediated protein aggregation required porphyrin-photosensitized singlet oxygen and porphyrin carboxylate side-chain deprotonation, and occurred with site-selective native protein methionine oxidation. Noncovalent interaction of protoporphyrin-IX with oxidized proteins led to protein aggregation that was reversed by incubation with acidified n-butanol or high-salt buffer. Phototoxicity and the ensuing proteotoxicity, mimicking porphyria photosensitivity conditions, were validated in cultured keratinocytes. Protoporphyrin-IX inhibited proteasome function by aggregating several proteasomal subunits, and caused cell growth arrest and aggregation of key cell proliferation proteins. Light-independent synergy of protein aggregation was observed when porphyrin was applied together with glucose oxidase as a secondary peroxide source.

CONCLUSIONS: Photo-excitable porphyrins with deprotonated carboxylates mediate protein aggregation. Porphyrin-mediated

proteotoxicity in the absence of light, as in the liver, requires porphyrin accumulation coupled with a second tissue oxidative injury. These findings provide a potential mechanism for internal organ damage and photosensitivity in porphyrias. (*Cell Mol Gastroenterol Hepatol* 2019;8:659–682; <https://doi.org/10.1016/j.jcmgh.2019.05.010>)

Keywords: Porphyria; Oxidative Stress; Amino Acid Oxidation; Phototoxicity.

Porphyrins are cyclic tetrapyrrole ligands found across all life forms. Porphyrins have a metal coordinating center that can be occupied by metals, including zinc in Zn-protoporphyrin-IX (Zn-PP) and iron in heme (Figure 1A). Heme biosynthesis is an 8-step enzymatic process, spanning mitochondrial and cytosolic compartments. The first step starts in the mitochondria, with glycine and succinyl Co-A forming δ -aminolevulinic acid (ALA), the first committed metabolite of the pathway.^{1–4} ALA then exits the mitochondria to the cytosol where it is successively converted into uroporphyrin (Uro), and then coproporphyrin (Copro), which enters the mitochondria to be converted to protoporphyrin-IX (PP-IX). Subsequently, PP-IX is converted to heme by ferrochelatase, which inserts iron into PP-IX.^{1,2} Notably, liver is the second largest source of heme (15%) after bone marrow (80%), with the remaining 5% being found in kidney and other organs.⁴ Heme precursor (eg, Uro, Copro, and PP-IX) accumulation is toxic and, when uncontrolled, results in pathologic conditions termed *porphyrias*.

Porphyrias are diseases characterized by excess porphyrin accumulation resulting from genetic defects in the heme biosynthetic pathway leading to 8 disorders, and they also may be caused by secondary porphyrin accumulation.^{3–5} Although the type of accumulating porphyrin, the organs affected, and the clinical manifestations vary depending on the porphyria, photosensitivity is a relatively common manifestation. Indeed, 6 porphyrias are associated with dermatologic involvement including erosive photodermatitis and/or acute painful photosensitivity.⁴ Notably, accumulations of Uro, Copro, or PP-IX in different combinations and proportions are reported in photosensitivity-associated porphyrias. Given that the liver is the second largest source of heme biosynthesis, it is not surprising that several porphyrias also have hepatic manifestations. For example, different degrees of liver damage are a common feature of hepatic porphyrias as in ALA-dehydratase porphyria, acute intermittent porphyria, and variegate porphyria.^{3,4,6–15} In addition, in cutaneous or extrahepatic porphyrias such as X-linked protoporphyria and erythropoietic protoporphyria, the source of porphyrin is primarily bone marrow, but liver also accumulates significant excess porphyrin, which leads to hepatic dysfunction.^{3,4,6–15} The extent of liver damage varies, with a small subset of patients developing end-stage liver disease requiring liver transplantation.¹⁶ For example, 5% of patients with erythropoietic protoporphyria develop acute hepatic insufficiency.¹⁷ The current model for porphyrin-mediated cytotoxicity


proposes that reactive oxygen species (ROS) generated through type I/II photosensitized reactions of porphyrins causes cell damage.^{16,18,19} This explains the severe photosensitive reactions observed in several porphyrias, but does not account for the internal organ damage that also is observed in some porphyria patients.

Although porphyrias have been studied since reported by Schultz in 1874,^{20,21} the mechanisms by which porphyrins mediate their toxicity are not clearly understood. Recently, in vitro and in vivo porphyrinogenic models showed the ability of porphyrins to induce proteotoxic stress and cause organelle-specific protein aggregation.^{22–24} In addition to protein aggregation, porphyrin accumulation also leads to nuclear ultrastructural alteration, endoplasmic reticulum (ER) damage, and proteasomal inhibition.^{23,24} PP-IX-mediated protein aggregation occurs via direct interaction of the porphyrin with its protein target as shown for lamin A/C, but it is not known if this binding is covalent.^{22,23}

There is remarkable specificity in the protein aggregation pattern depending on the source and type of porphyrin. For example, ER proteins are more susceptible to endogenously triggered porphyrinogenic stress, whereas intermediate filament (IF) proteins (eg, cytoplasmic keratins and nuclear lamins) are more prone to aggregation upon exogenous porphyrinogenic stress.²³ The selectivity of porphyrin–protein interactions is highlighted further by the observation that known porphyrin-binding proteins do not aggregate under similar experimental conditions. For example, liver fatty acid binding protein 1, an abundant cytosolic protein that binds PP-IX,²⁵ does not aggregate upon PP-IX accumulation.²³ Similarly, the mitochondrial translocator protein that also binds with PP-IX²⁶ is unaffected by porphyrin treatment.²³ The relative selectivity of the porphyrin-mediated protein aggregation targets led us to propose that porphyria-associated tissue damage is caused in part by porphyrin-mediated protein aggregation.^{22–24}

Protein aggregation and inclusion body formation is a hallmark of several pathologic conditions including neurodegenerative diseases,²⁷ alcoholic and nonalcoholic steatohepatitis, chronic cholestasis, metabolic disorders, and hepatocellular neoplasms.²⁸ In the current work, we tested the hypothesis that porphyrin-mediated protein aggregation

Abbreviations used in this paper: ¹O₂, singlet oxygen; ALA, δ -aminolevulinic acid; BCA, Bicinchoninic acid; Copro, coproporphyrin; DDC, 3,5-diethoxycarbonyl-1,4-dihydrocollidine; DFO, deferoxamine; DMA, dimethylacetamide; EPR, electron paramagnetic resonance spectroscopy; ER, endoplasmic reticulum; GOX, glucose oxidase; HMW, high molecular weight; IF, intermediate filament; K, keratin; MS, mass spectrometry; Met, methionine; NP-40, Nonidet P-40; O₂⁻, superoxide; PAGE, polyacrylamide gel electrophoresis; PBS, phosphate-buffered saline; POBN, α -(4-pyridyl-1-oxide)-N-tert-butylinitrone; PP-Dim, protoporphyrin-IX dimethyl ester; PP-IX, protoporphyrin-IX; ROS, reactive oxygen species; RPN1, 26S proteasome regulatory subunit RPN1; SDS, sodium dodecyl sulfate; TMPD, N, N, N', N'-tetramethyl-p-phenylenediamine; Uro, uroporphyrin; Zn-PP, zinc protoporphyrin-IX.

 Most current article

© 2019 The Authors. Published by Elsevier Inc. on behalf of the AGA Institute. This is an open access article under the CC BY-NC-ND license (<http://creativecommons.org/licenses/by-nc-nd/4.0/>).

2352-345X

<https://doi.org/10.1016/j.jcmgh.2019.05.010>

occurs through direct interaction of porphyrin with aggregation-prone proteins, via a mechanism that requires ambient light and oxygen, or in the absence of light but via a secondary oxidative stress insult.

Results

Deprotonated Propionate Side Chains of PP-IX Are Essential for Porphyrin-Mediated Protein Aggregation

To identify molecular features of the porphyrin molecule that may be required for protein aggregation, we used a cell-free protein aggregation assay whereby lysates of Huh7 cells (human hepatocellular carcinoma cells), were used to test the effect of different porphyrin derivatives on the formation of high molecular weight (HMW) aggregates of selected proteins.²³ Use of the cell lysate allowed us to test the effect of cell-impermeable porphyrins, such as Uro and Copro (Figure 1A), on proteins that are highly susceptible to porphyrin-mediated aggregation (eg, keratin [K]8 and K18, lamin A/C, lamin B1). As shown in Figure 1B–G, exposure of Huh7 lysates to PP-IX at pH 7.4 led to marked K8, K18, lamin A/C, and lamin B1 aggregation. Chelation of PP-IX with iron (to generate heme) led to minimal aggregation, while Zn-PP retained its protein aggregating ability. Of note, Zn-PP is fluorescent whereas hemin is not. Thus, metallating the tetrapyrrole porphyrin maintains its aggregation capacity as long as the chelated product is photo-excitabile.

Next, we tested whether the vinyl carbon or the propionate side chain play a role in the observed protein aggregation. Deuteroporphyrin-IX (which lacks the vinyl carbon chain) (Figure 1A) resulted in similar protein aggregation compared with PP-IX, whereas, in contrast, PP-IX dimethyl ester (PP-Dim) dramatically decreased protein aggregation (Figure 1B–G). This indicates that the ionizable propionic side chain but not the methyl esterification is essential for PP-IX-mediated protein aggregation. Uro and Copro (which have 8 and 4 COOH, respectively) (Figure 1A) showed similar protein aggregation compared with PP-IX (which has 2 COOH), thereby suggesting a positional effect of the COOH group or an effect related to the extent of ionization of the Uro and Copro derivatives at pH 7.4 compared with PP-IX. To further confirm the role of ionizability of the propionic acid side chain (acid dissociation constant [pKa] [stronger acidic] = 3.68; pKa [weaker acidic] = 4.96; data retrieved from Human Metabolome Database), we mixed the Huh7 lysate with PP-IX at pH 4.5 to protonate, and pH 8.9 to deprotonate, the propionic acid side chain. Compared with pH 7.4, pH 4.5 abolished the protein aggregating ability of PP-IX, whereas pH 8.9 resulted in marked aggregation (Figure 1B–G). Hence, a photo-excitabile tetrapyrrole with a deprotonated propionic acid side chain is essential for protein aggregation. This phenomenon was observed for several proteins, namely K8, K18, lamin A/C, and lamin B1. We validated these finding by assessing protein aggregation in intact Huh7 cells using the cell-permeable porphyrin derivatives PP-IX, Zn-PP, and PP-Dim (Figure 2).

PP-IX-Mediated Protein Aggregation Requires Oxygen

Because the established paradigm in the field is that porphyrin-mediated cytotoxicity involves porphyrin-sensitized generation of ROS and free radicals,^{4,29} we tested whether PP-IX-mediated ROS formation is important for protein aggregation. Huh7 cell lysates were treated with PP-IX under ambient O₂ concentration (~300,000 ppm) or in an anoxic chamber (~5 ppm). Anoxic conditions virtually abolished the ability of PP-IX to cause protein aggregation (Figure 3A), which shows the pivotal role played by O₂ in porphyrin-mediated protein aggregation. To identify potential ROS involvement in PP-IX-mediated protein aggregation, PP-IX treatment was performed with or without different excited state or ROS scavengers (Figure 3B–G). The ROS scavengers used (and their targets) included N,N,N',N'-tetramethyl-p-phenylenediamine (TMPD) (singlet state), sodium azide (singlet oxygen, ¹O₂), mannitol (hydroxyl radical), superoxide dismutase/catalase (superoxide, O₂⁻), and trolox (¹O₂ and singlet state). The singlet state and singlet oxygen scavenging markedly diminished PP-IX-mediated K8, K18, lamin A/C, and lamin B1 aggregation, while scavenging O₂⁻ and hydroxyl radical had no effect (Figure 3B–G). Thus, as reported earlier, porphyrins transition between ground to singlet and triplet states,³⁰ however, as our results show, subsequent generation of ¹O₂ appears to be required for PP-IX-mediated protein aggregation.

In addition to generating singlet oxygen, there is a potential for PP-IX to form radicals that could play a role in protein aggregation. To test this hypothesis, we used electron paramagnetic resonance spectroscopy (EPR) on PP-IX-treated cell lysate with α -(4-pyridyl-1-oxide)-N-tert-butyl-nitron (POBN) as a spin trap. PP-IX alone showed 2 distinct EPR signals (Figure 3H, boxes marked with a dotted line labeled I and II), whereas the lysate alone showed no signal. Incubating the lysate with PP-IX increased the I and II signal amplitudes in addition to a third signal (Figure 3H, box III), consistent with radical formation. The hyperfine coupling constants for hydrogen (aH) and nitrogen (aN) in the (PP-IX) + (lysate) spectrum were approximately 2.9 and 15.6 Gauss, respectively. These values are similar to those observed for other POBN radical adducts.³¹ As expected, treatment of the lysate-PP-IX mix with NaN₃ markedly dampened the EPR signal amplitude. In summary, we envision a cascade whereby porphyrin in the ground state absorbs light energy and transitions to a triplet/singlet state. The higher energy state then decays back to the ground state, and the released extra energy is taken up by O₂ to form ¹O₂, which then leads to protein aggregation through a radical-mediated process.

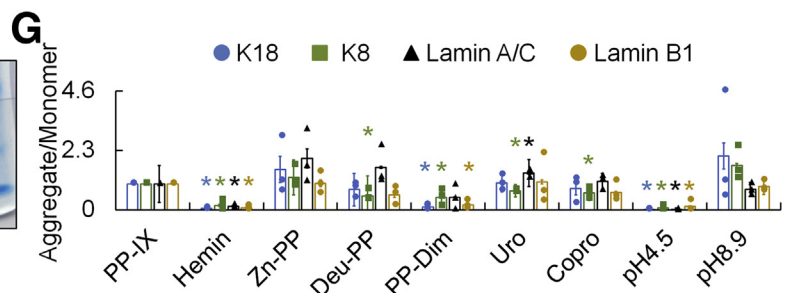
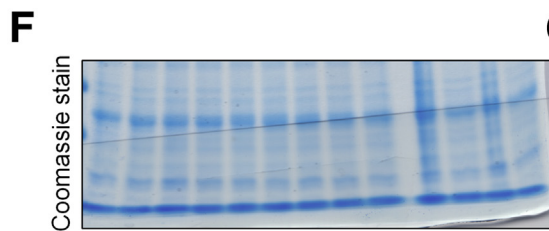
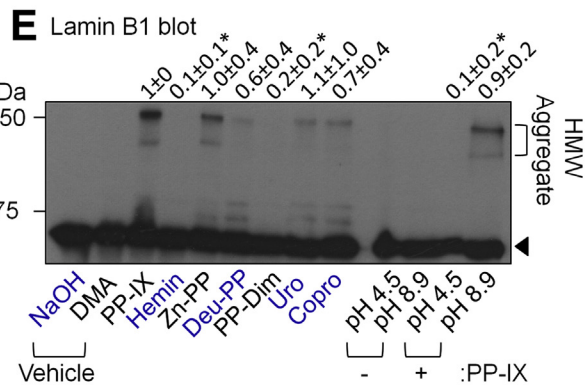
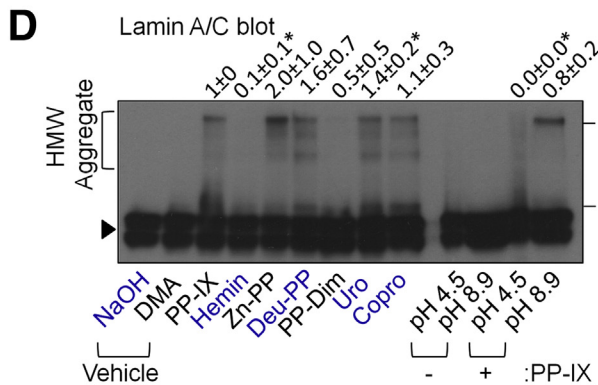
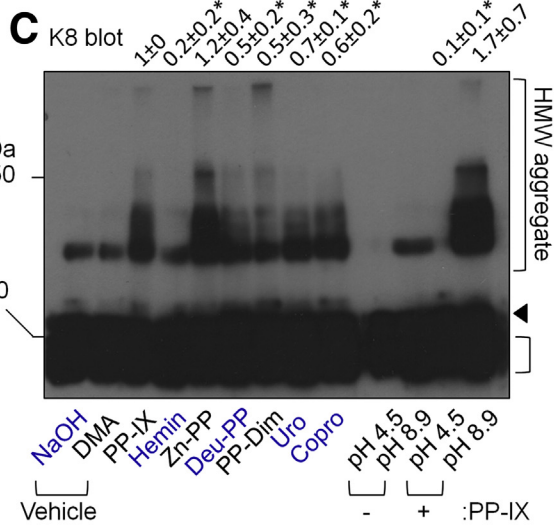
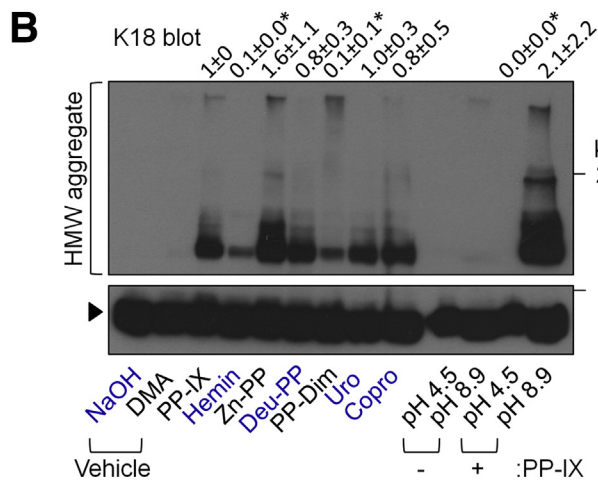
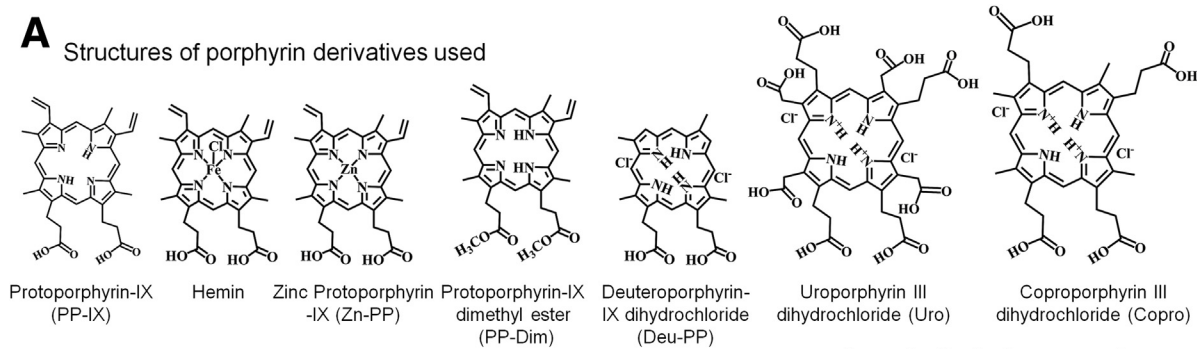
Noncovalent Porphyrin-Protein Interaction and Native Protein Targets Are Required for PP-IX-Mediated Protein Aggregation

Our results show that the protein-aggregating ability of PP-IX is highly dependent on the finer details of its structure (Figure 1), and its protein-aggregating ability cannot be

attributed to the porphyrin's ROS generating capacity alone. For example, the protein-aggregating ability of PP-Dim is markedly less than PP-IX, however, as for PP-IX, PP-Dim also generates ROS³² and is a better photosensitizer

compared with PP-IX.³³ This led us to hypothesize that to mediate protein aggregation, porphyrins need to physically interact with the aggregation-prone proteins in their native forms. To test this hypothesis, we denatured Huh7 cell

A Structures of porphyrin derivatives used



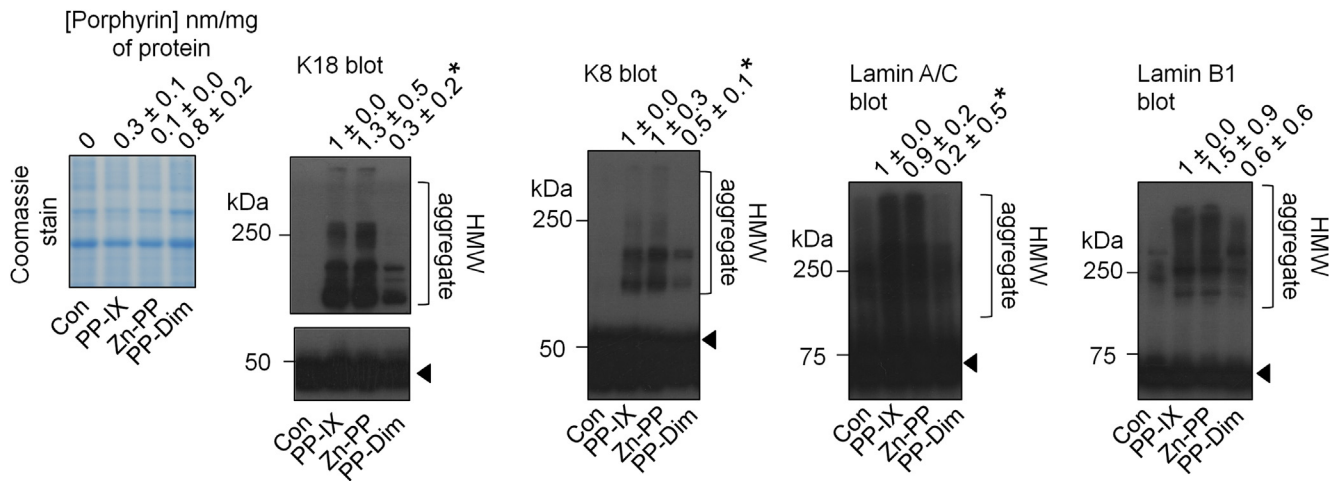


Figure 2. PP-IX dimethyl ester does not cause protein aggregation in Huh7 cells. Huh7 cells were treated with the indicated porphyrin derivatives (5 $\mu\text{mol/L}$, 1 h) followed by blotting using the indicated antibodies (data are representative of 3 independent experiments, and the monomer bands are marked with *arrowheads*). The scanned aggregate/monomer ratio (shown at the *top* of the blot) is the average of 3 samples \pm SD; statistical significance ($*P < .05$) was determined using an unpaired *t* test (2-tailed) compared with PP-IX-treated cells. The porphyrin levels (*top* of the Coomassie stain lanes) are an average of 3 samples \pm SD.

lysates by heating (95°C, 3 min) or by using 2% sodium dodecyl sulfate (SDS) and then treated the lysates with PP-IX in ambient light and compared aggregation with non-denatured lysates treated with PP-IX. There was significant protection from aggregation in the denatured lysates (especially with 2% SDS) that is readily visualized by Coomassie staining (Figure 4A, dotted box) and by immunoblotting of K8, K18, lamin A/C, and lamin B1 (Figure 4B–E).

To show direct protein–porphyrin interaction, we monitored in-gel (using native polyacrylamide gels) porphyrin fluorescence of porphyrin-treated cell lysates in ambient light or dark conditions with or without heat denaturing the lysates (Figure 4F and G). Free PP-IX migrated as a discrete visible band (Figure 4F, arrowhead), and did not fluoresce in the ethidium bromide channel (Figure 4G). As expected, the lysate alone did not show any visible fluorescence signal, but when the lysate was incubated with PP-IX there was a dramatic change in the PP-IX signal. The discrete PP-IX banding pattern (observed under visible light) disappeared completely, and a prominent fluorescent smearing pattern appeared under UV light. Notably, the porphyrin–protein interaction under dark conditions that do not cause SDS–polyacrylamide gel

electrophoresis (PAGE)–detectable HMW protein aggregation (Figure 4H and I) or of heat-denatured lysate (Figure 4A–E) does not change protein–PP-IX interaction (Figure 4F and G). This indicates that PP-IX binding to proteins changes its fluorescence property, irrespective of the folded state of the proteins, and leads to PP-IX fluorescence (as noted in the ethidium bromide channel). The data also show that PP-IX protein interaction is stronger in the presence of light because it leads to SDS–PAGE–resistant protein aggregates, whereas in dark binding it is detectable only under native gel conditions and does not manifest as SDS–PAGE–resistant HMW aggregates (Figure 4F–I).

We then tested the nature of the porphyrin–protein interaction, and whether PP-IX extraction, using high-salt or the acidified organic solvent n-butanol, alters the porphyrin-mediated protein aggregation. The protein aggregation systems we examined were Huh7 cells treated with PP-IX or liver extracts of mice fed the porphyrinogenic compound 3,5-diethoxycarbonyl-1, 4-dihydrocollidine (DDC). Both extraction methods were highly effective in removing the PP-IX from the cell and liver homogenates, with the organic solvent being more effective, without loss in protein recovery (Figure 4J and K). Importantly, there

Figure 1. (See previous page). Specific structural motifs of porphyrins modulate porphyrin-mediated protein aggregation. (A) Structures of porphyrin derivatives used in this study. (B–E) Huh7 cell lysate (0.5 mg protein/mL in 400 mmol/L phosphate buffer, pH 7.4) was treated with 25 $\mu\text{mol/L}$ of the indicated porphyrin derivatives, or corresponding solvent vehicle (NaOH labeled in blue, and DMA). For assessing the pH effect (last 4 lanes to the *right*), the reaction mixture was prepared in 400 mmol/L NaH_2PO_4 (pH 4.5) or 400 mmol/L Na_2HPO_4 (pH 8.9). After porphyrin treatment, the proteins were separated by SDS–PAGE, followed by blotting with the indicated antibodies. The data are representative of 3 independent experiments, and the monomer bands are marked with an *arrowhead*. The unlabeled bracket ‘]’ in panel C denotes cross-reactivity of K8 antibody with K18. (F) Coomassie staining of 1 duplicate gel of those used for blotting in panels B–E, the gel is included to show near-equal protein loading. (G) Densitometry scanning of the bands in panels B–E was performed using ImageJ software to quantify the aggregate/monomer band intensity ratio (normalized to 1 in the PP-IX-treated samples). Error bars represent SD ($n = 3$ experiments); statistical significance was determined using an unpaired *t* test (2-tailed). $*P < .05$ and denotes comparison with PP-IX. The mean aggregate/monomer ratio \pm SD ($n = 3$) also is shown at the top of the blots.

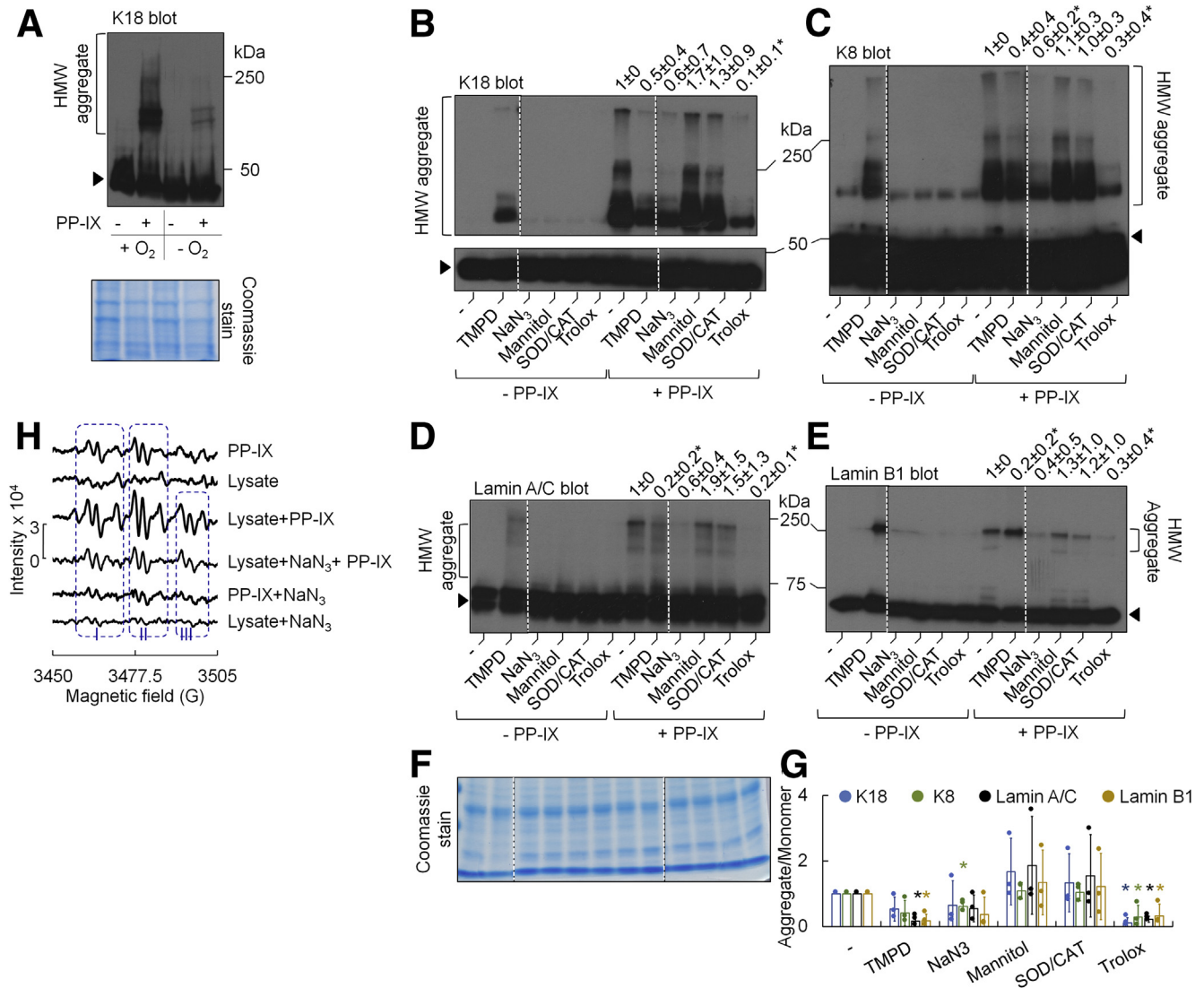


Figure 3. PP-IX-mediated protein aggregation requires oxygen. (A) Huh7 cell protein lysates (2 mg/mL) were treated with 100 $\mu\text{mol/L}$ PP-IX (30 min, 37°C) under ambient atmospheric and light conditions (+O₂) or inside an anoxic chamber (-O₂). After treatment, the proteins were blotted with anti-K18 antibody. (B–E) Huh7 cell lysate (as in Figure 1B–E) was treated with PP-IX (25 $\mu\text{mol/L}$, 30 min, 37°C, in light conditions), in the presence or absence of the indicated excited state/free radical scavengers. Lysates then were blotted with the indicated antibodies. The data are representative of 3 independent experiments. Samples to the left and right of the dotted lines were analyzed on the same gel (monomer bands are highlighted by arrowheads). Where shown as separate panels (B), the monomer (lower panel) was exposed for 5 seconds, whereas the HMW aggregates (upper panel) were exposed for 5 minutes. (F) Coomassie staining of a typical gel used in panels B–E is included to show similar protein loading. (G) Densitometry scanning of the bands in panels B–E was performed using ImageJ software to quantify the aggregate/monomer band intensity ratios (normalized to 1 in the PP-IX-treated samples). Error bars represent SD ($n = 3$ experiments); statistical significance was determined using an unpaired t test (2-tailed). * $P < .05$ and denotes comparison with PP-IX. The mean aggregate/monomer ratio \pm SD ($n = 3$) also is shown at the top of the blots in panels B–E. (H) Huh7 cell lysate (4 mg protein/mL) was treated with 200 $\mu\text{mol/L}$ of PP-IX (supplemented with 20 mmol/L NaN₃, where indicated; all samples included 36 mmol/L of POBN) for 15 minutes, and continuous-wave EPR spectra were collected. The dotted lines highlight the EPR peaks (boxes I–III).

was a marked decrease in the level of residual K18 HMW aggregates after porphyrin extraction (Figure 4L and M), and a similar trend was observed for K8 and lamins (Figure 5). Thus, in the presence of light and O₂, PP-IX interacts preferentially with proteins in their native conformation through noncovalent ionic and hydrophobic interactions and leads to protein aggregation.

Porphyrin Phototoxicity in Keratinocytes Involves Organelle Selective Protein Aggregation

Because several genetic porphyrias show severe photosensitivity,⁴ we tested whether porphyrin accumulation and subsequent protein aggregation extends to keratinocytes. We used N/Tert keratinocytes, which are normal human keratinocytes immortalized by transfection to express TERT.^{34,35}

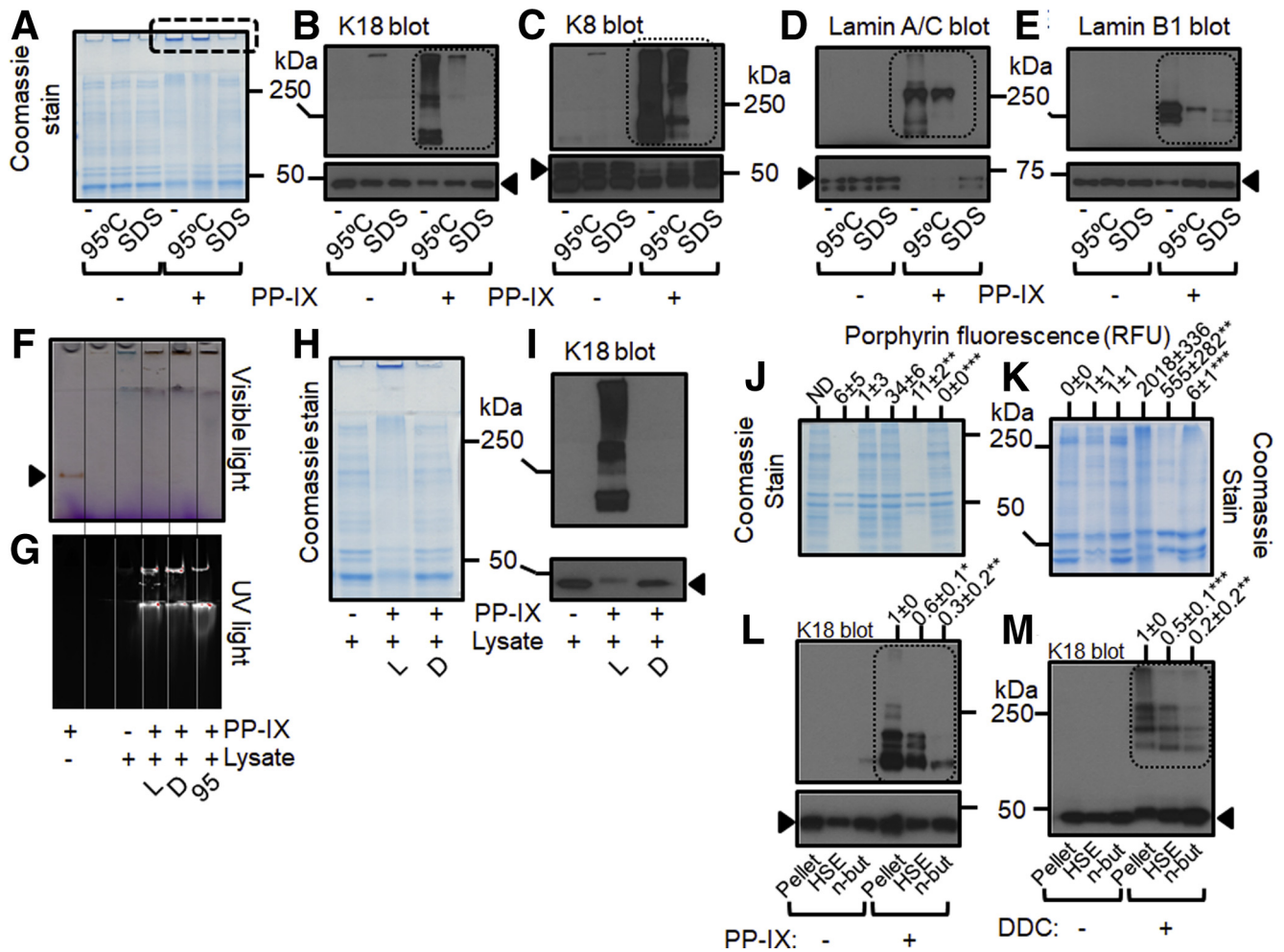


Figure 4. Porphyrins bind preferentially with proteins in their native conformation through noncovalent interaction to cause protein aggregation. (A–E) Huh7 cell lysate (0.5 mg protein/mL) was denatured by heating (95°C, 3 min) or with 2% SDS, and then treated with 25 $\mu\text{mol/L}$ PP-IX (30 min, ambient light conditions). Samples then were separated by SDS-PAGE and visualized by (A) Coomassie staining and (B–E) blotted with the indicated antibodies. The data are representative of 3 independent experiments, and the monomer bands are marked with arrowheads. (F and G) Huh7 cell lysate (4 mg protein/mL) was treated with 200 μM PP-IX in light (L) or dark (D) conditions, or after heat denaturing by heating at 95°C for 3 minutes (processing of samples in dark were done as described before²³). Samples were separated using native PAGE, and then scanned under (F) visible or (G) UV light. (H and I) An aliquot of lysate from the experiment described in panels F and G was separated using SDS-PAGE and (H) visualized by Coomassie staining, and (I) then blotted with anti-K18 antibody. (I) Arrowhead points to monomeric K18 (film was exposed for 5 s), whereas the HMW aggregate film (upper panel) was exposed for 5 minutes. (J–M) Porphyrins were extracted from (J and L) Huh7 cells that were pretreated with 5 $\mu\text{mol/L}$ PP-IX for 1 hour, or from (K and M) livers of C57BL/6 male mice fed DDC for 5 days, using high salt extraction (HSE) or acidified n-butanol (n-but), and compared with the unextracted pellet sample (pellet) as detailed in the *Materials and Methods* section. (J and K) After extraction, the residual porphyrin was measured, and the porphyrin fluorescence was normalized to the cellular protein content and expressed as an average of 3 independent experiments \pm SD (top). (J) $**P = .003$, $***P = .0005$ denote comparison with pellet with added PP-IX, and was determined using an unpaired t test (2-tailed). (K) $**P = .005$, $***P = .0005$ denote comparison with pellet with added PP-IX, and was determined using an unpaired t test (2-tailed). Proteins were separated by SDS-PAGE and visualized by (J and K) Coomassie staining and (L and M) blotting with anti-K18 antibody. Monomer bands are marked by arrowheads, and the data are representative of 3 independent experiments. (L and M) Densitometry scanning of the bands was performed using ImageJ software to quantify the aggregate/monomer band intensity ratio (normalized to 1 before extraction of the porphyrin). Error bars represent SD ($n = 3$ experiments); statistical significance was determined using an unpaired t test (2-tailed). (L) $*P = .02$, $**P = .002$. (M) $***P = .0007$, $**P = .001$ denotes comparison with pellet (+PP-IX or +DDC).

To mimic porphyria-associated photosensitivity, we treated the keratinocytes with PP-IX (5 $\mu\text{mol/L}$, 1 h), or overnight with ALA (1 mmol/L) and deferoxamine (DFO, 100 $\mu\text{mol/L}$). One set of cells was completely shielded from light during PP-IX or ALA + DFO treatment (labeled as D), while the samples labeled as L were exposed to ambient light during

treatment through usual incubator door opening and closing. After harvesting, both sets were processed in the dark. As expected, light exposure did not have an appreciable effect in porphyrin accumulation (Figure 6A, porphyrin measurements are shown at the top of the Coomassie-stained lanes). Notably, porphyrin accumulation in light-exposed cells

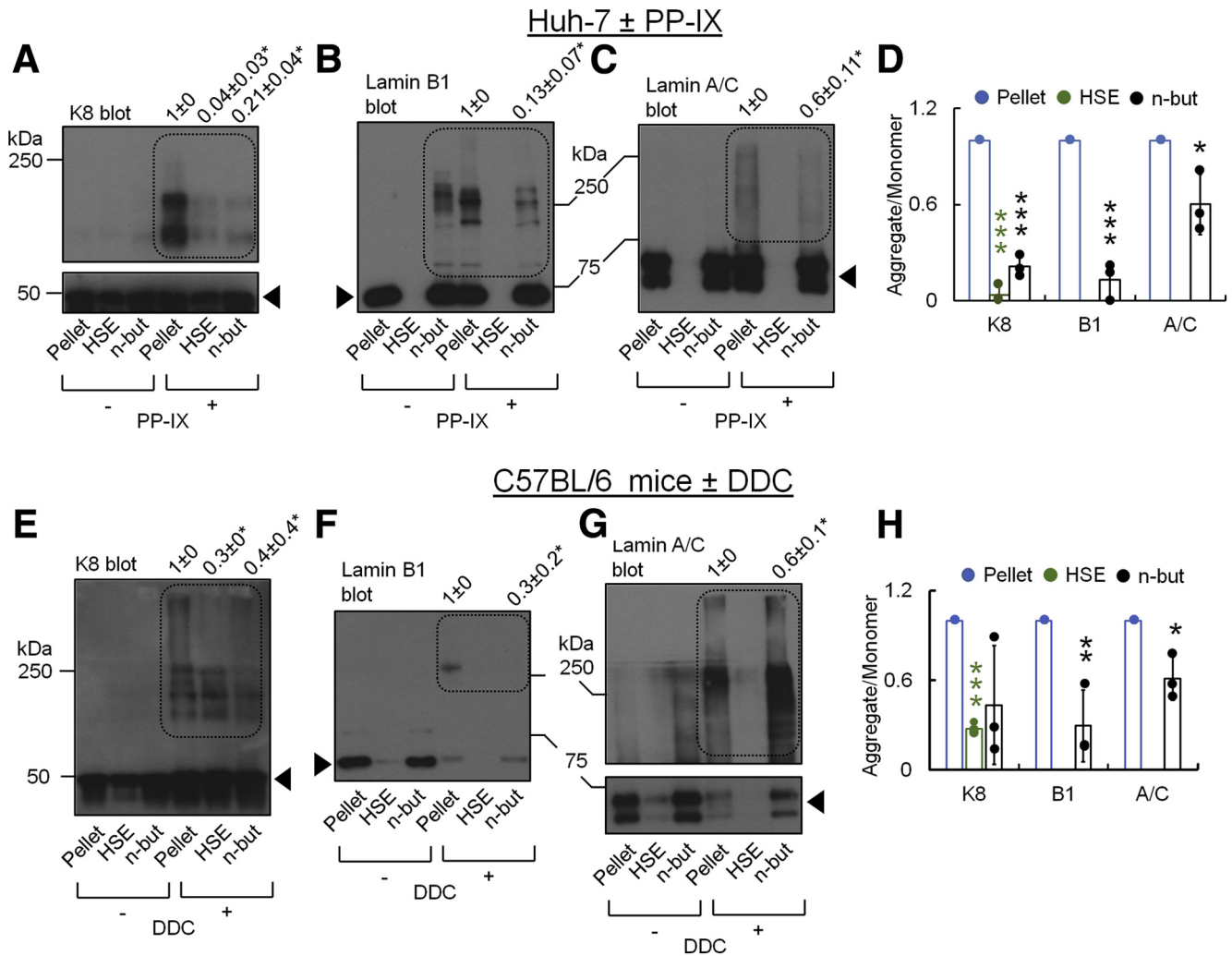


Figure 5. Porphyrin extraction reverses SDS-PAGE–detected aggregation of K8 and lamins A/C and B1. (A–D) Huh7 lysates (same as used in Figure 4J and L) and (E–H) lysates from livers of DDC-fed mice (same as used in Figure 4K and M) were separated by SDS-PAGE and blotted with the indicated antibodies. Arrowheads highlight the monomer bands. (D and H) Densitometry scanning of the bands (shown in blots A–C for panel D, and shown in blots E–G for panel H) was performed using ImageJ software to quantify the aggregate/monomer band intensity ratios. The aggregate/monomer ratio in the +PP-IX or +DDC pellet samples was normalized to 1. (D and H) The error bars represent SD (n = 3 experiments); statistical significance was determined using an unpaired *t* test (2-tailed). (D) ****P* < .0005, **P* = .02 denotes comparison with pellet (+PP-IX). (H) ****P* = .0001, ***P* = .007, **P* = .01 denotes comparison with pellet (+DDC). As expected, HSE samples do not show any Lamin A/C or B1 bands.

resulted in protein aggregation in several cell compartments (nucleus [lamin A/C], cytoplasm [K5], ER [protein disulfide isomerase; Figure 6B, C]). In addition, several components of the protein clearance machinery such as p62 and ubiquitinated proteins were aggregated and accumulated, respectively (Figure 6). Importantly, because the light-exposed samples also were dark-processed, the organelle-specific protein aggregation was not caused by a processing artifact from cell content intermixing after cell lysis.

PP-IX Oxidizes the Hydrophobic Residues of the Heptad Coiled-Coil Motif of IF Proteins

Because PP-IX generates $^1\text{O}_2$ and radicals in the presence of protein (Figure 3), we tested whether PP-IX-mediated

protein aggregation leads to oxidation of select amino acids within the protein backbone. We focused on the IF proteins keratins and lamins, given their susceptibility to PP-IX-mediated protein aggregation (Figure 1). Mass spectrometry (MS) analysis of PP-IX-treated Huh7 cells was performed as detailed in the *Materials and Methods* section. Given that $^1\text{O}_2$ plays an important role in porphyrin-mediated protein aggregation (Figure 3), we undertook a targeted approach and searched the collected MS data to selectively examine $^1\text{O}_2$ -mediated amino acid oxidations that have been reported previously.^{36,37} The abundance of the peptides with oxidized amino acids were normalized to the total peptide content of each protein. For the IF proteins we tested, a significant increase in oxidized methionine residues compared with vehicle-treated cells was

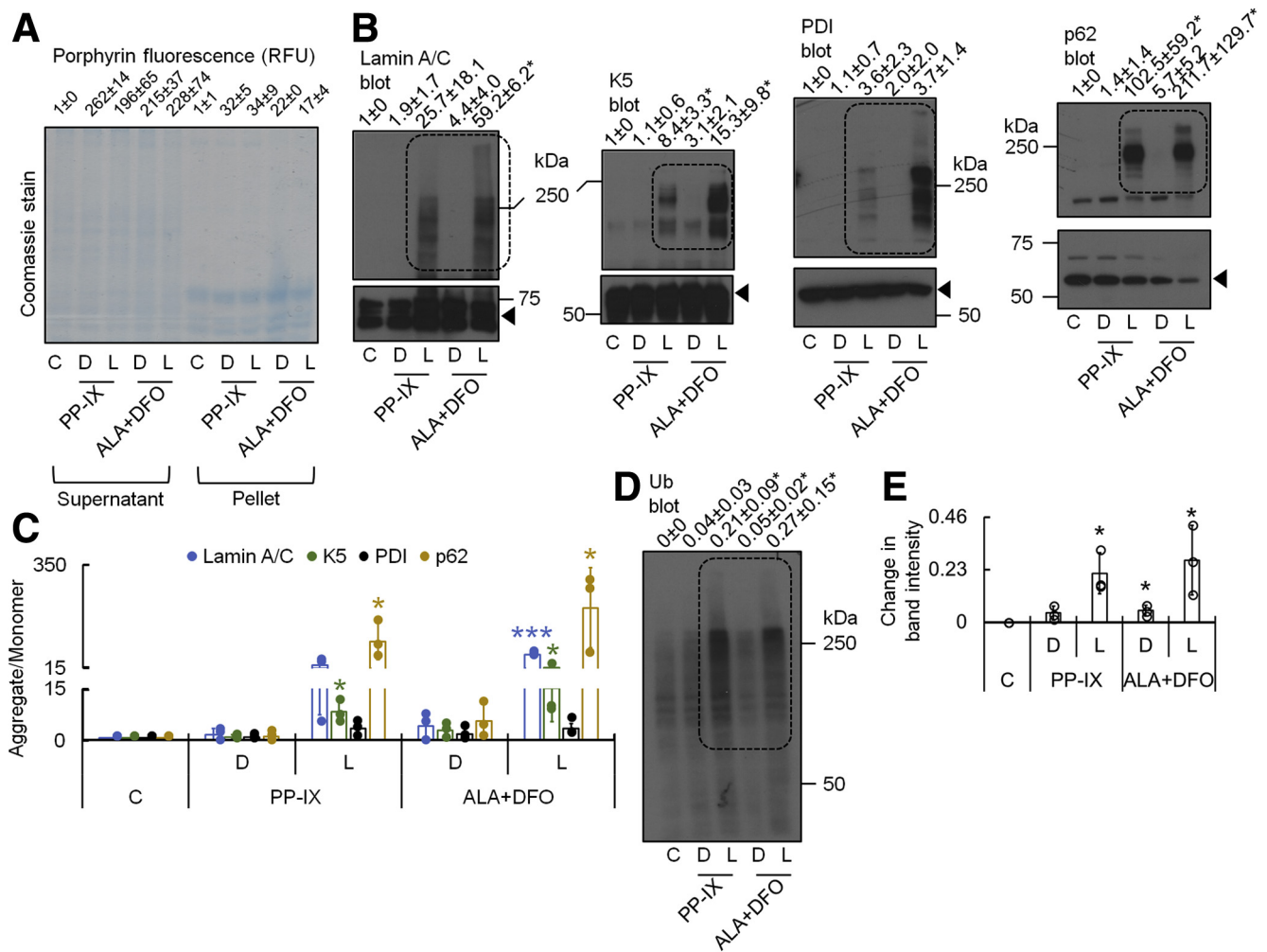


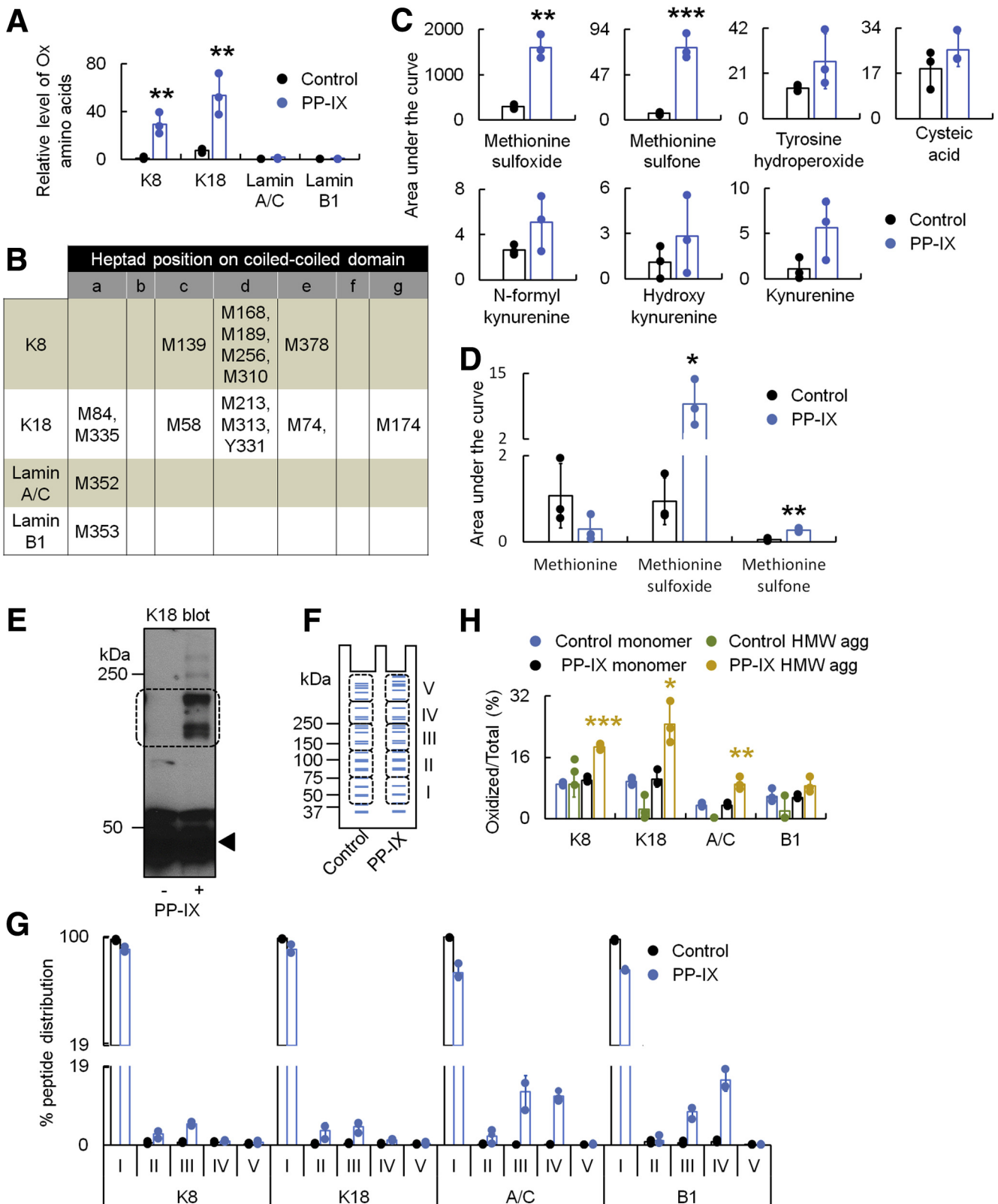
Figure 6. Porphyrin-mediated phototoxicity in cultured keratinocytes leads to protein aggregation. (A and B) Human N/Tert keratinocytes were treated in light (L) or dark (D) conditions with PP-IX (1 h) or with ALA + DFO (overnight) and compared with control cells (C). The cells then were processed in the dark, which entailed protein isolation and separation using SDS-PAGE under reducing conditions and blotting with antibodies to the indicated antigens. Porphyrin levels were normalized to cellular protein content and averaged from 2 independent experiments \pm SD (shown above the Coomassie stain in panel A). The *dotted windows* highlight the HMW aggregates, and the *arrowheads* denote the monomers. Coomassie staining is included as loading control. The data shown in panel B is representative of 3 independent experiments. (C) Densitometry scanning of the bands in panel B was performed using ImageJ software to quantify the aggregate/monomer band intensity ratio (the control sample [C] was normalized to 1). Error bars represent SD ($n = 3$ experiments), and statistical significance was determined using an unpaired t test (2-tailed). * $P < .05$, and denotes comparison with control. (D and E) Ubiquitin blot of the lysates used in panel B; the difference in band intensity between control (C) and PP-IX- or ALA + DFO-treated cells is shown in panel E. Error bars represent SD ($n = 3$ experiments), and statistical significance was determined using an unpaired t test (2-tailed). * $P < .05$ and denotes comparison with control. The mean aggregate (*dotted box*) to monomer ratio \pm SD ($n = 3$, panels B and D) is shown at the *top* of the blot, and the mean band intensity change \pm SD ($n = 3$, panel E) is shown. PDI, protein disulfide isomerase; RFU, Relative Fluorescence Unit.

observed (particularly for keratins as compared with lamins) (Figure 7A and B). An important structural feature of IF proteins is that their central coiled-coil α -helix motif that consists of 310–350 amino acid heptad repeats represented as $(a-b-c-d-e-f-g)_n$, where residues a and d are typically hydrophobic and residues b , c , e , f , and g often are charged.³⁸ Mapping of the oxidized residues showed that the majority are at positions a and d (Figure 7B). Notably, for lamin A/C (M352) and B1 (M353), these residues were the only ones significantly oxidized and they shared the motif ³⁵²MQQQ and ³⁵³MQQQ, respectively.

Because IF proteins are not the only proteins that aggregate upon porphyrin accumulation,²³ we expanded the proteomic analysis to the entire Huh7 proteome. Relative quantitation of the oxidized amino acid products after PP-IX treatment showed dramatic increases in methionine (Met)-sulfoxide and Met-sulfone in PP-IX-treated samples (Figure 7C). Although tyrosine hydroperoxide and cysteine acid levels did not change appreciably, tryptophan oxidation products (n-formylkynurenine, hydroxyl-kynurenine, and kynurenine) increased in PP-IX-treated cells (Figure 7C) as noted upon using purified peptides,³⁷ but the changes were

not statistically significant. Because methionine was the most susceptible amino acid to PP-IX-mediated oxidation, we validated our findings by analyzing free methionine oxidation patterns in cell-free Huh7 lysates treated with

PP-IX. Free methionine decreased 4-fold after PP-IX treatment commensurate with a concomitant increase in the formation of Met-sulfoxide (9-fold) and Met-sulfone (5-fold) (Figure 7D).



To further delineate the role of oxidation, we analyzed the extent of protein oxidation in aggregated vs monomeric species after PP-IX treatment. To test this hypothesis, we treated Huh7 cells with PP-IX and validated protein aggregation by immunoblotting for K18 (Figure 7E, dotted region). Next, we used an MS-based proteomic approach to test proteins from 3 independent sets of control and PP-IX-treated samples whereby the SDS-PAGE separated lanes were divided into areas I-V (Figure 7F). The proteins were eluted from the different gel regions, digested with trypsin, and then analyzed by MS. The percentage of peptide abundance in the different segments of the lanes showed that K8 and K18 HMW aggregates were present predominantly in regions II and III, whereas lamins A/C and B1 HMW aggregates were detected in regions III and IV (Figure 7G). There was a significantly higher proportion of oxidized K8, K18, and lamin A/C peptides in the HMW aggregates of PP-IX-treated cells (Figure 7H).

Next, we tested how protein denaturation (which abrogates PP-IX-aggregating potential) (Figure 4A-E) alters PP-IX-mediated protein oxidation. Huh7 cell lysates were pre-denatured (either by heating for 3 minutes at 95°C or with 2% SDS), treated with PP-IX, and compared with PP-IX treatment of native proteins. MS (Figure 8) allowed us to quantify the abundance of peptides from proteins with oxidized amino acids in PP-IX-treated denatured vs native samples as detailed in the *Materials and Methods* section. Figure 8A shows the plot of $-\log_{10}(P \text{ value})$ vs the ratio of Ox-denatured to Ox-native peptides. Of the 43,200 peptides identified by MS, 2753 peptides were oxidized after PP-IX treatment (Figure 8C). The oxidation level of the majority of the peptides did not change significantly when comparing denatured PP-IX and native PP-IX samples, but there was a fraction (253 peptides) that were significantly less oxidized when the proteins were denatured by 2% SDS. Notably, 169 peptides were oxidized only when the native proteins were treated with PP-IX, but not when they were pre-denatured by SDS ("unique to native") (Figure 8C). A small subset of peptides showed increased oxidation in the samples that were pre-denatured, which

could be attributed to protein unfolding and increased access to PP-IX-generated $^1\text{O}_2$. A similar trend for K18 was observed when the samples were heat denatured, then treated with PP-IX, and compared with native proteins treated with PP-IX (Figure 8D-F). K8 and lamin A/C showed similar trends (Figure 9). These findings highlight the selectivity of PP-IX-mediated protein oxidation and how it is guided by the conformation of the susceptible proteins. Therefore, PP-IX appears to selectively oxidize specific residues in aggregation-prone proteins, and the oxidized proteins coalesce by noncovalent PP-IX protein interactions to form the HMW aggregates that are resistant to SDS-PAGE separation.

PP-IX Serves as a Persistent Source of Oxidants and Does Not Undergo Rapid Autoxidation

Earlier studies have shown that porphyrin-generated $^1\text{O}_2$ causes intramolecular self-oxidation of the porphyrin ring.³⁹⁻⁴¹ Because photosensitized PP-IX causes protein oxidation, we tested whether PP-IX becomes autoxidized in the protein PP-IX reaction mixture. To address this question, we treated Huh7 cell lysate (adjusted to 0.5 mg/mL protein) with 50 $\mu\text{mol/L}$ PP-IX. The control reaction mixture consisted of 50 $\mu\text{mol/L}$ PP-IX mixed with the lysate buffer. After extraction with methanol, PP-IX was analyzed by liquid chromatography MS and ultra-performance liquid chromatography with UV detection. Compared with PP-IX alone, the PP-IX protein reaction mixture showed no decrease in the PP-IX amount, as judged by the positive ion-mode $(M + H)^+$ 563 signal that corresponded to PP-IX alone (Figure 10A-C). In addition, no new masses were observed in the PP-IX protein reaction mixture (Figure 10D and E). Analysis of the UV chromatogram at 400 nm (absorbance maxima for PP-IX) did not show any new peaks in the PP-IX protein reaction mixture (Figure 10F-H). Therefore, PP-IX preferentially oxidizes the proteins it binds to without significant autoxidation in the time frame of the experiment. This suggests that PP-IX may serve as a persistent, nearly catalytic source of oxidants.

Figure 7. (See previous page). PP-IX-mediated protein aggregation involves amino acid oxidation. Huh7 cells were treated with 5 $\mu\text{mol/L}$ PP-IX for 1 hour and processed as detailed in the *Materials and Methods* section. (A) Relative level of oxidized amino acid residues, normalized to the total peptide content. The error bars represent SD ($n = 3$ experiments); statistical significance was determined using an unpaired t test (2-tailed). $**P < .006$ and denotes comparison with control. (B) Position of the oxidized amino acids in the heptad motifs of K8, K18, and lamins A/C and B1. (C) Relative quantitation of oxidized amino acids in the entire proteome of PP-IX-treated Huh7 cells. The area under the curve for peptides with the indicated modifications was normalized to the total area under the curve for all the peptides detected. Error bars represent SD ($n = 3$ experiments); statistical significance was determined using an unpaired t test (2-tailed). $**P = .001$, $***P = .0008$ and denotes comparison with control. (D) Relative quantitation of free Met, Met sulfoxide, and Met sulfone in PP-IX-treated Huh7 cells, as calculated from the area under the curve, normalized to protein content. Error bars represent SD ($n = 3$ experiments); statistical significance was determined using an unpaired t test (2-tailed). $*P = .04$, $**P = .002$ and denotes comparison with control. (E) Huh7 cell lysates were blotted with anti-K18 antibody; the region of the Coomassie-stained gel is marked with dotted boxes (dotted line represents K18 aggregates and arrowhead denotes monomer). The blot is representative of 3 independent experiments. (F) Cell extracts (\pm PP-IX as in panel E) were separated by SDS-PAGE followed by MS-based identification of the proteins in regions I-V of the gel with a focus on K8, K18, and lamins A/C and B1. (G) Percentage of peptide distribution of K8, K18, and lamins A/C and B1 in regions I-V of the gel in control vs PP-IX-treated samples. The data are the average of 3 independent experiments with error bars representing SD. (H) Proportion of abundance of peptides with oxidized residues to total peptides for the indicated proteins (control or PP-IX-treated) from monomer or HMW-aggregated regions of the Coomassie gel. The error bars represent SD ($n = 3$ experiments), and statistical significance was determined using an unpaired t test (2-tailed). $*P = .013$, $**P = .004$, and $***P = .001$ and denotes comparison with PP-IX-treated monomer. agg, aggregate.

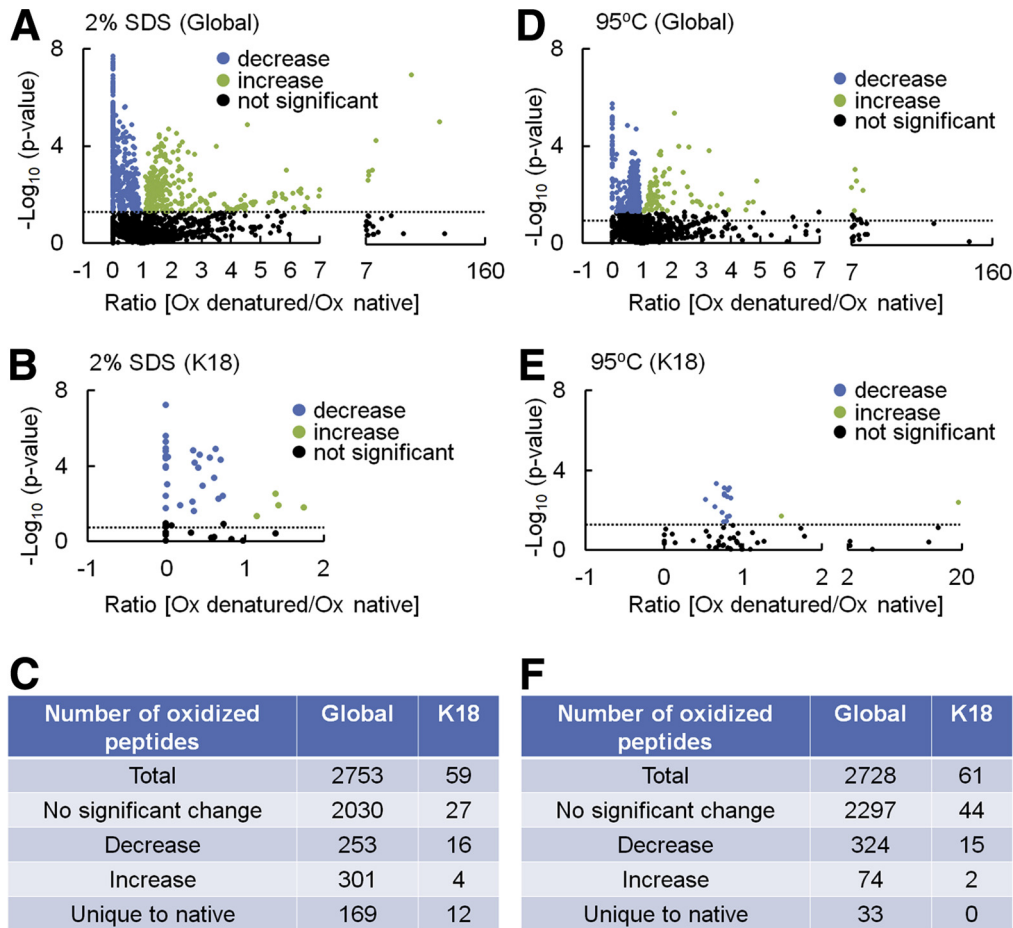


Figure 8. Protein denaturation decreases PP-IX-mediated protein oxidation. Huh7 cell extracts were denatured using 2% SDS or heating to 95°C, or were treated as is (native) with PP-IX. (A, B, D, and E) The distribution plots of $-\text{Log}_{10}(P \text{ value})$ vs ratio (Ox denatured/Ox native) for all of the oxidized peptides, or for K18, as identified by MS, are shown as labeled. The dotted line intersects the y-axis at 1.3, which corresponds to $P = .05$, thus the data points under the dotted line are not statistically significant. A summary of the data is shown in for the (C) SDS treatment and for the (F) 95°C treatment. The data shown are averaged from 3 independent experiments.

Light-Independent Protein Aggregation by Porphyrins

Protein oxidation is a key process in PP-IX-mediated protein aggregation, and the oxidant ($^1\text{O}_2$) is formed by light-sensitized PP-IX; although in the absence of light there is no oxidant formation, and hence barely detectable HMW aggregate formation that is resistant to SDS-PAGE separation. We hypothesized that if a secondary source of ROS were provided, porphyrins would be able to induce protein aggregation even in the absence of light. To test this hypothesis, we treated Huh7 with 12.5–50 mU/mL of glucose oxidase (GOX) as a source of hydrogen peroxide for 24 hours in the presence or absence of ALA + DFO. Exposure to GOX alone induced protein aggregation, particularly at higher concentrations (Figure 11A–E), but co-treatment of GOX with ALA + DFO increased protein aggregation in both dark and light conditions (light > dark) for K8 and K18 (Figure 11A, B, E, and G). For aggregation-prone proteins that had cysteine residues (eg, lamin B1), analysis also was performed under nonreducing SDS-PAGE. Lamin B1 showed GOX/ALA + DFO synergy only under nonreducing but not under reducing conditions (Figure 11C and D). This highlights the significant effect that PP-IX has on protein

conformation because protein interaction with PP-IX likely increased access to GOX-generated hydrogen peroxide by possibly unfolding lamin B1, as quantified by the aggregate to monomer ratio as a function of GOX concentration (Figure 11F and G). Increasing GOX concentration led to a linear increase in aggregate/monomer ratios for the 4 proteins tested (K8, K18, lamin A/C, and lamin B1), with an additive effect of ALA+DFO (light > dark), manifested as increased y-intercept and slope (ALA + DFO, light > ALA + DFO, dark > control) (Figure 11G). Hence, in the presence of a secondary source of ROS, porphyrin accumulation promotes protein aggregation independent of light.

PP-IX Inhibits the Proteasome by Preferential Aggregation of Proteasome Regulatory Particle Subunits

Previously, we showed that porphyrin inhibits the peptidase activity of the proteasome in liver extracts obtained from DDC-fed mice,⁴² and in lysates of cultured cells pretreated with PP-IX or ALA + DFO.²³ We hypothesized that PP-IX-mediated proteasome inhibition involves proteasomal subunit aggregation. To test this hypothesis,

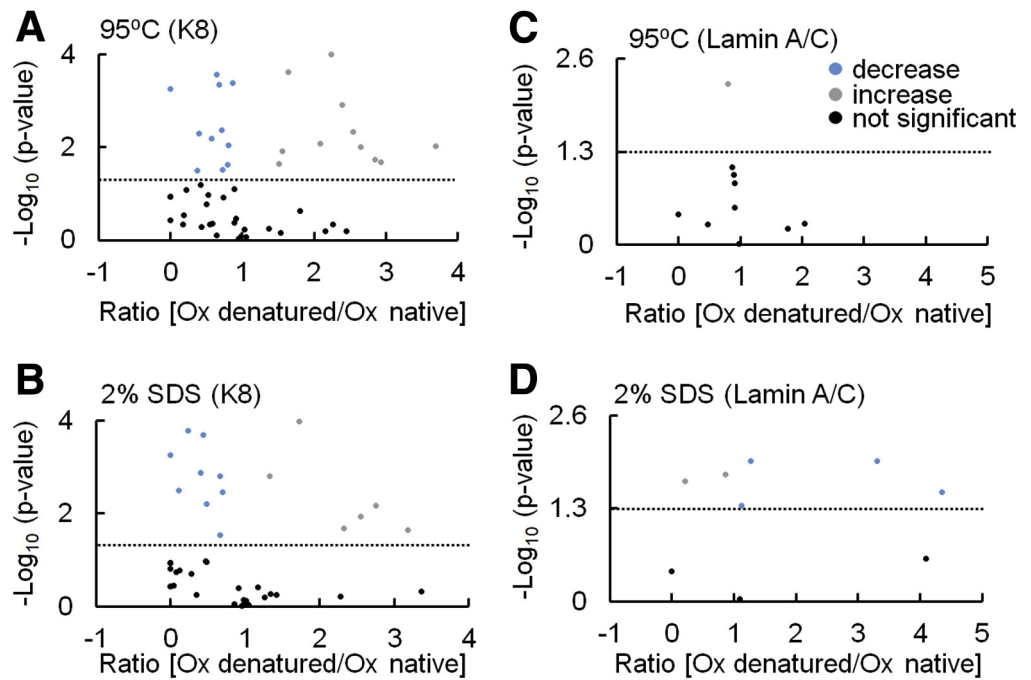


Figure 9. Native conformation is required for PP-IX-mediated protein oxidation in K8 and lamin A/C. Samples were analyzed as described for Figure 8. The distribution plots of $-\text{Log}_{10}$ (P value) vs ratio (Ox denatured/Ox native) of (A and B) K8 and (C and D) lamin A/C oxidized peptides identified by MS (average of 3 independent experiments are shown). The samples were denatured by heating at 95°C or by 2% SDS, then treated with PP-IX and compared with native proteins treated with PP-IX. The dotted line intersects the y-axis at 1.3, which corresponds to $P = .05$; thus data points under the dotted line are not statistically significant. (E) The table summarizes the data shown in panels A–D.

Number of oxidized peptides	K8		Lamin A/C	
	95°C	2% SDS	95°C	2% SDS
Total	50	49	10	10
No significant change	27	27	9	3
Decrease	10	13	1	2
Increase	12	6	0	5
Unique to native	1	3	0	0

using lysates from the experiment described in Figure 7E–G, we validated proteasome inhibition by the accumulation of ubiquitinated proteins (Figure 12A, dotted region). Next, we used the same MS-based proteomic approach and samples described in Figure 7E–G to test whether proteasome subunits were aggregated upon exposure to PP-IX. Proteins from control and PP-IX-treated samples were separated using reducing SDS-PAGE conditions, and the lanes were divided into areas I–V (Figure 7F). Proteins that were detected in a region higher than its known molecular weight were considered to be aggregated. For example, monomeric RPN5 (53 kilodaltons) was detected solely in region I in control samples, whereas RPN5 was detected primarily in the higher regions II and III only in PP-IX-treated samples (Figure 12B). Notably, 6 proteasome subunits belonging to the 19S regulatory particle and 1 proteasome-associated scaffold protein (proteasome adapter and scaffold protein Ecm29) were aggregated as judged by their prominent abundance in HMW aggregate forms (Figure 12C). We validated these finding using immunoblotting by showing decreased RPN1 monomer antibody reactivity after PP-IX treatment (Figure 12D and E). Long exposure of the

radiograph film (Figure 12D) did not detect HMW aggregates. We have observed this phenomenon previously in other proteins such as lamin B1 (eg, Figure 10 in Maitra et al²³), which we attribute to loss of antibody reactivity to the target antigen resulting from epitope masking by oxidation and/or aggregation. To further show this phenomenon of antibody epitope masking, we treated Huh7 cell lysates with 5, 25, and 125 $\mu\text{mol/L}$ of PP-IX followed by immunoblotting of the proteins using anti-p62 antibody (Figure 12F). Lower concentrations of PP-IX (5 $\mu\text{mol/L}$) led to loss of p62 monomer and concomitant formation of HMW aggregates. Increasing the PP-IX concentration to 25 and 125 $\mu\text{mol/L}$ still caused monomer loss, but the HMW aggregate level did not increase appreciably, thereby highlighting the decrease in antibody reactivity to markedly aggregated forms of the protein. Thus, loss of the 26S proteasome regulatory subunit RPN1 monomer antibody reactivity likely reflects a surrogate indirect assessment of protein aggregation after PP-IX treatment given the validation by MS, which showed RPN1 peptides in higher regions of the gel. Collectively, PP-IX accumulation inhibits the homeostatic machinery of the proteasome by selective aggregation of its subunit particles.

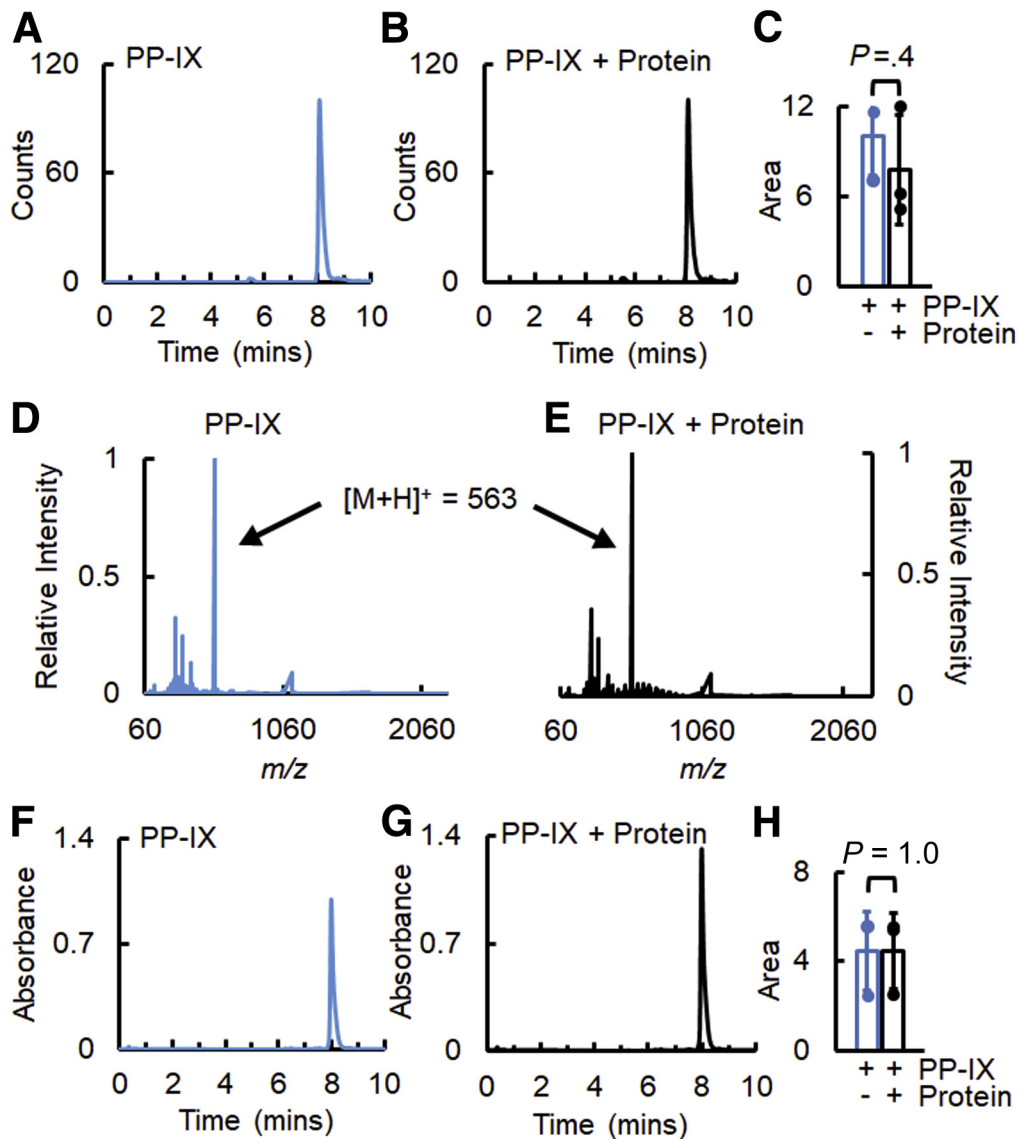


Figure 10. PP-IX does not undergo rapid self-sensitized oxidation. (A and B) PP-IX alone (50 $\mu\text{mol/L}$) was compared with 50 $\mu\text{mol/L}$ PP-IX incubated with Huh7 cell lysate (adjusted to 0.5 mg/mL protein). The reaction mixtures were analyzed by liquid chromatography–MS, and ultra-performance liquid chromatography with UV detection. The extracted ion chromatogram for $(M + H)^+ 563$ shows the PP-IX content. The data are representative of 3 independent experiments. (C) Quantification of the area under curve for the $(M + H)^+ 563$ peak (average of 3 independent experiments with error bars representing SD). Statistical significance was determined using an unpaired *t* test (2-tailed). (D and E) Mass spectrum of the eluents from 8 to 8.3 minutes, corresponding to the PP-IX peaks shown in panels A and B. (F and G) Chromatogram recorded at 400 nm for the PP-IX and PP-IX + protein reaction mixtures. (H) Quantification of the area under the curve for the PP-IX peak shown in panels F and G. The data are an average of 3 independent experiments with error bars representing SD. Statistical significance was determined using an unpaired *t* test (2-tailed).

Porphyrin Accumulation Abolishes the Proliferative Capacity of Huh7 Cells

To further assess the effect of protein aggregation on cellular homeostasis, we examined the effect of ALA + DFO on Huh7 cell growth and cell cycle progression. As expected, cells treated with ALA + DFO manifested a time-dependent increase in porphyrin accumulation (Figure 13A). Porphyrin accumulation correlated with a lack of cell growth because Trypan blue exclusion staining of the cells showed that ALA + DFO-treated

cells did not show cell death, although their cell numbers did not increase (Figure 13B). Cell-cycle analysis showed that control cells grew asynchronously as expected, and the ALA + DFO-treated cells did not manifest appreciable changes in the G0/G1, S, and G2/M cell fractions (Figure 13C and D). These cell cycle profiles were commensurate with a significant decrease in antibody reactivity to proliferating cell nuclear antigen (essential for DNA replication and repair⁴³), cyclin B1 (essential for mitosis⁴⁴), and cyclin-dependent kinase 4

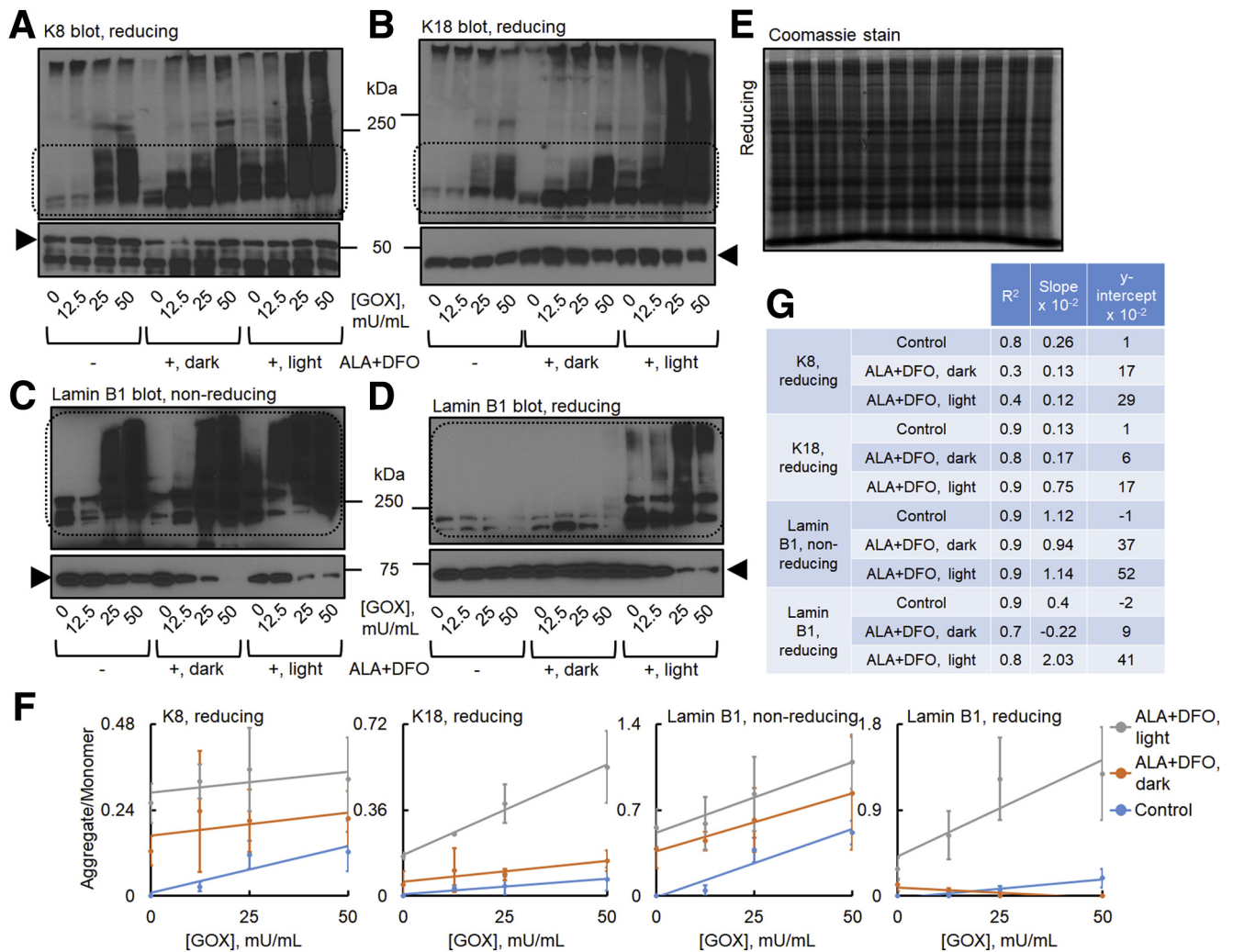


Figure 11. Synergistic effect of porphyrin accumulation and GOX-mediated oxidative stress. (A–D) Huh7 cells were treated with GOX (12.5, 25, 50 mU/mL) for 24 hours, alone or together with ALA + DFO, in light or in dark conditions. The proteins then were isolated from the cells and separated by SDS-PAGE under reducing or non-reducing conditions, and then blotted with antibodies to the indicated proteins. (E) A Coomassie stain is included to show near-equal loading of the protein samples. (F) Quantification of the band intensities, performed by ImageJ. For the immunoblots, the monomer bands are marked with *arrowheads* and the films were exposed for 5 seconds, whereas the films for the HMW aggregates (*upper panels*) were exposed for 15 minutes. The data shown in the blots are representative of 3 independent experiments, and the data shown in panel F represent an average of 3 independent experiments, with the error bars representing standard error of measurement. (G) Summary of the linear regression analysis of the different samples shown in panel F.

(essential for G1-phase progression⁴⁵) (Figure 14). In addition, ubiquitinated proteins accumulated in ALA + DFO-treated cells (Figure 14G and H). Hence, PP-IX accumulation after ALA + DFO treatment caused cell growth arrest that likely was due to PP-IX-mediated aggregation of key proteins involved in cell proliferation and cell-cycle progression.

Discussion

Porphyrin-Mediated Protein Aggregation Is Reversible

Our results highlight the pivotal role of low pH and protonation of the PP-IX propionate side chain in blocking

PP-IX-mediated protein aggregation. This suggests that deprophyrination and lack of, or limited, aggregation in the acidic compartments of autophagolysosomes might reverse porphyrin-protein aggregation, thereby potentially restoring a functional protein pool unless protein oxidation of the monomer interferes with its function. Indeed, porphyrin accumulation in zebrafish induces autophagy, possibly to mitigate the proteotoxic stress,²⁴ while activating autophagy by rapamycin decreases DDC-induced protein inclusion body formation.⁴⁶ Thus, inducing autophagy and/or deprophyrination and disaggregation may provide a potential therapeutic strategy in porphyria-associated tissue damage, as occurs in photosensitive skin lesions.

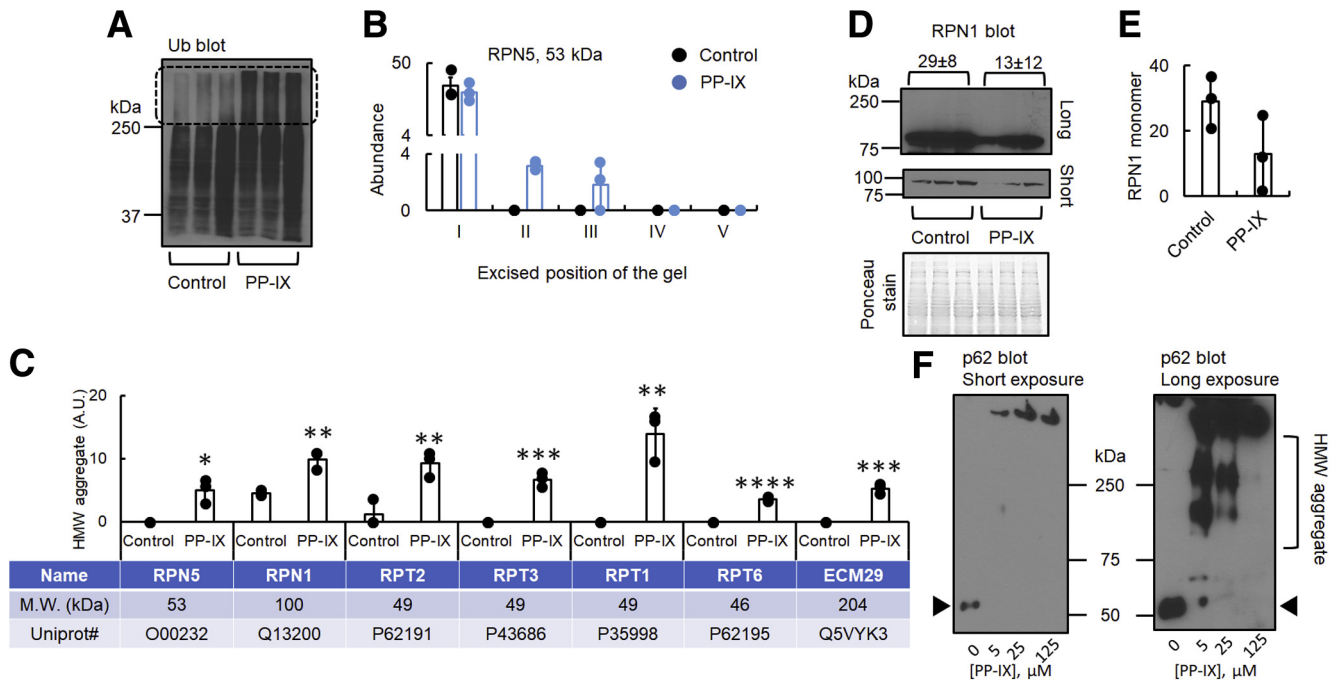


Figure 12. PP-IX inhibits the proteasome by aggregating select proteasomal subunits. (A) Huh7 cells were treated with PP-IX for 1 hour followed by blotting the cell lysates with anti-ubiquitin antibody. (B) Cell extracts (\pm PP-IX treatment from panel A) were separated by SDS-PAGE followed by MS-based identification of proteins in regions I–V of the gel, as performed in Figure 7, with a focus on proteasome subunits. Distribution of RPN5 peptides in regions I–V of the gel in control vs PP-IX-treated samples is shown. The data are the average of 3 independent experiments with error bars representing SD. (C) Histogram summarizing the abundance of proteasome subunits and proteasome-associated proteins detected as HMW aggregates by MS in PP-IX-treated vs control cells. Proteins that were detected in a region higher than their known molecular weights were considered to be aggregated. The data are the average of 3 independent experiments with error bars representing SD. Statistical significance was determined using an unpaired *t* test (2-tailed). **P* = .01, ***P* < .009, ****P* < .0006, and *****P* = .00009 denotes comparison with control. (D) Aliquots from the samples in panel A were separated by SDS-PAGE and then blotted with anti-RPN1 antibody. The lower panel (labeled Short) denotes a 3-minute exposure of the film, and the upper panel (labeled Long) denotes overnight exposure. A Ponceau stain of the membrane is included to show similar loading of the samples. (E) Quantification of the monomer band intensity of RPN1 using the Short exposure film. The data were averaged from 3 independent experiments, with error bars representing the standard error of measurement. The monomer band intensity \pm SD (*n* = 3) also is shown at the top of the blot. (F) Huh7 cells were solubilized in 1% NP-40, and the soluble protein fraction was adjusted to 1 mg/mL followed by treatment with 5, 25, 125 μ mol/L of PP-IX. Proteins then were separated by SDS-PAGE (reducing conditions) and blotted with anti-p62 antibody. The monomer bands are marked with arrowheads. A shorter (left panel) and longer exposure (right panel) of the same membrane is shown. MW, molecular weight.

The ROS Scavenger Choice Is Important for Preventing Porphyrin-Mediated Protein Aggregation

Although our current findings, as well as other studies, point to the role of ROS (eg, $^1\text{O}_2$) in porphyrias,^{5,47,48} antioxidant supplementation therapy (including β -carotene, N-acetyl-cysteine, vitamin C) has shown limited benefit.⁴⁹ This could be owing to reasons ranging from poor partitioning in the cytoplasmic compartment (eg, β -carotene) to poor scavenging ability of the specific ROS that is generated. As our data show, choosing the appropriate ROS scavenger (eg, trolox) is of paramount importance in preventing porphyrin-mediated protein aggregation. Trolox is a cell-permeable vitamin E derivative that efficiently protects from porphyrin-mediated protein aggregation. It may be possible to consider combination therapy in the context of porphyria-associated photosensitivity, such as using targeted ROS scavengers in addition to afamelanotide, with the

latter leading to increased production of eumelanin and a subsequent decrease in light penetrance.⁴⁷

Prophyrin-Protein Complexes Form an Intermolecular Sensitizer-Acceptor Couple

$^1\text{O}_2$ has an intracellular diffusion distance of 10–20 nm and a lifetime of 10–40 nanoseconds before it is quenched.^{36,50,51} In addition, the oxidation efficiency by $^1\text{O}_2$ has geometric constraints such as the 3-dimensional orientation of the potential targets around the source of $^1\text{O}_2$.⁵² The precise localization of the $^1\text{O}_2$ sensitizer (porphyrin) with respect to the acceptor (oxidizable amino acids in aggregation prone proteins) occurs only when there is porphyrin binding to the native protein with consequent protein aggregation. Protein denaturation disrupts the 3-dimensional orientation, so despite porphyrin binding there is no protein aggregation. Similar examples of coupling of an oxidant source to its targets was reported earlier. For example, myeloperoxidase (source of

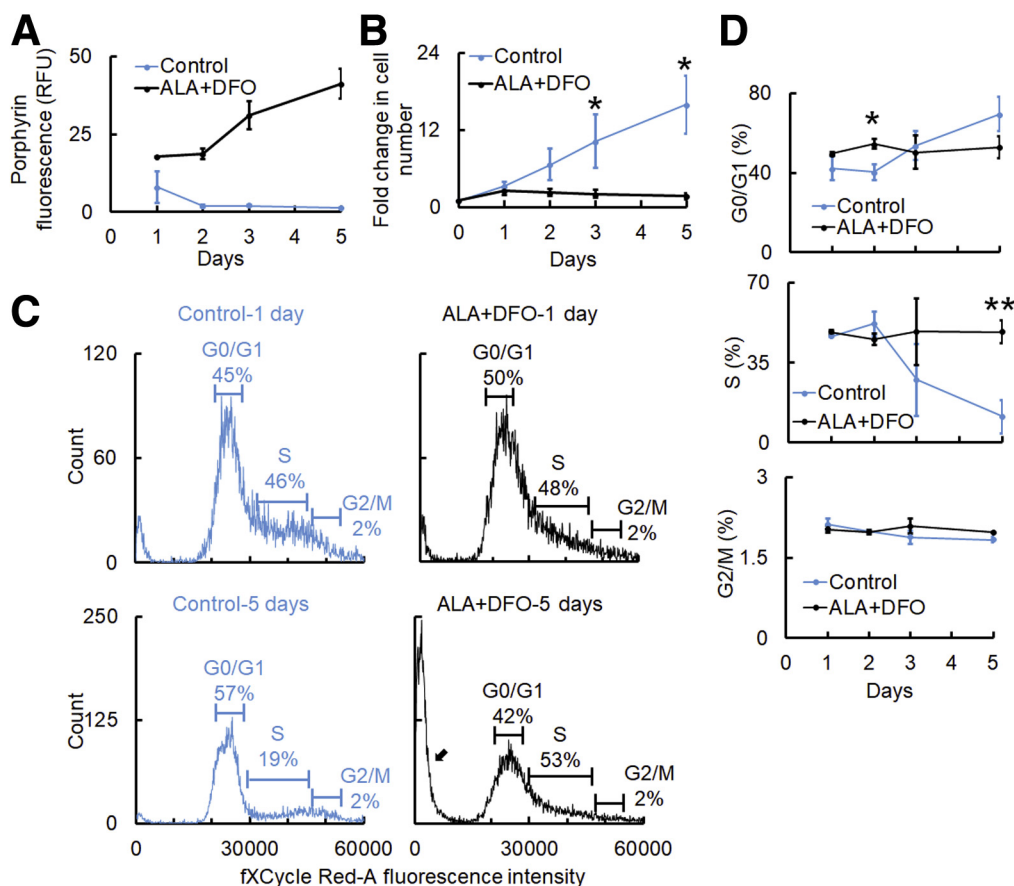


Figure 13. Porphyrin accumulation in response to ALA + DFO treatment causes arrest of cell growth. Huh7 cells (2.1×10^6) were seeded on a 150-mm plate on day 0, and after 1 day the medium was changed and ALA + DFO-containing media were added. Cells were harvested by trypsinization at the indicated days after ALA + DFO treatment. A duplicate dish without ALA + DFO was maintained similarly. (A) Cellular porphyrin levels (normalized to protein content). The data are the average of 3 independent experiments, with error bars representing standard error of measurement. (B) The number of viable cells (\pm ALA+DFO) after the indicated days, measured using Trypan blue exclusion. The number of cells that were plated was normalized to 1 to calculate the fold change in cell number (averaged from 4 independent experiments), with error bars representing the standard error of measurement; statistical significance was determined using an unpaired *t* test (2-tailed). **P* < .05 and denotes comparison with control. (C) Histograms show DNA content (x-axis, fluorescence intensity of the nuclear stain, fXCycle Red-A, ThermoFisher Scientific, Waltham, MA) and relative distribution of populations in different cell-cycle phases (y-axis) obtained as detailed in the *Materials and Methods* section. The data are representative of 3 independent experiments. (D) Quantification of the proportion of cells in different cell-cycle phases as a function of ALA + DFO treatment days. The data are an average of 3 independent experiments, with error bars representing the standard error of measurement. Statistical significance was determined using an unpaired *t* test (2-tailed). **P* = .04, ***P* = .007 and denotes comparison with control. RFU, Relative Fluorescence Unit.

the diffusible oxidant hypochlorous acid) binds to the oxidation target apoA-I moiety of high-density lipoprotein.⁵³ Singlet oxygen sources, including porphyrins, also may cause intramolecular self-oxidation of the porphyrin ring,^{39–41} but we did not detect measurable oxidized porphyrin products within the time frame of the analysis. Thus, porphyrin-protein interactions switch the balance of the interaction pathway overwhelmingly toward targeted intermolecular oxidation, which implies that intracellular porphyrins might act as a sustaining and catalytic source of singlet oxygen.

Oxidation of Select Amino Acids by Porphyrins

We tested the potential oxidation of amino acids in IF proteins because of their relative structural

conservation^{38,54–57} and their susceptibility to aggregation in the presence of porphyrins.^{22–24} Oxidation of residues *a/d* in the *a-g* heptad repeats of the IF coiled-coil α -helical rod domain, particularly methionines, suggests that structural considerations within the α -helical domain promote accessibility of these residues and lead to aggregation in a mechanism that remains to be defined. Small peptides with heptad motifs are known to form coiled-coil superhelical structures.⁵⁸ Covalently linked porphyrin-peptide conjugates are known to form supramolecular aggregates where the peptide molecule wraps around the hydrophobic porphyrin macrocycle.^{59,60} For example, a peptide comprising 3 contiguous heptad motif repeats self-assembled to form millimeter scale fibrils when incubated

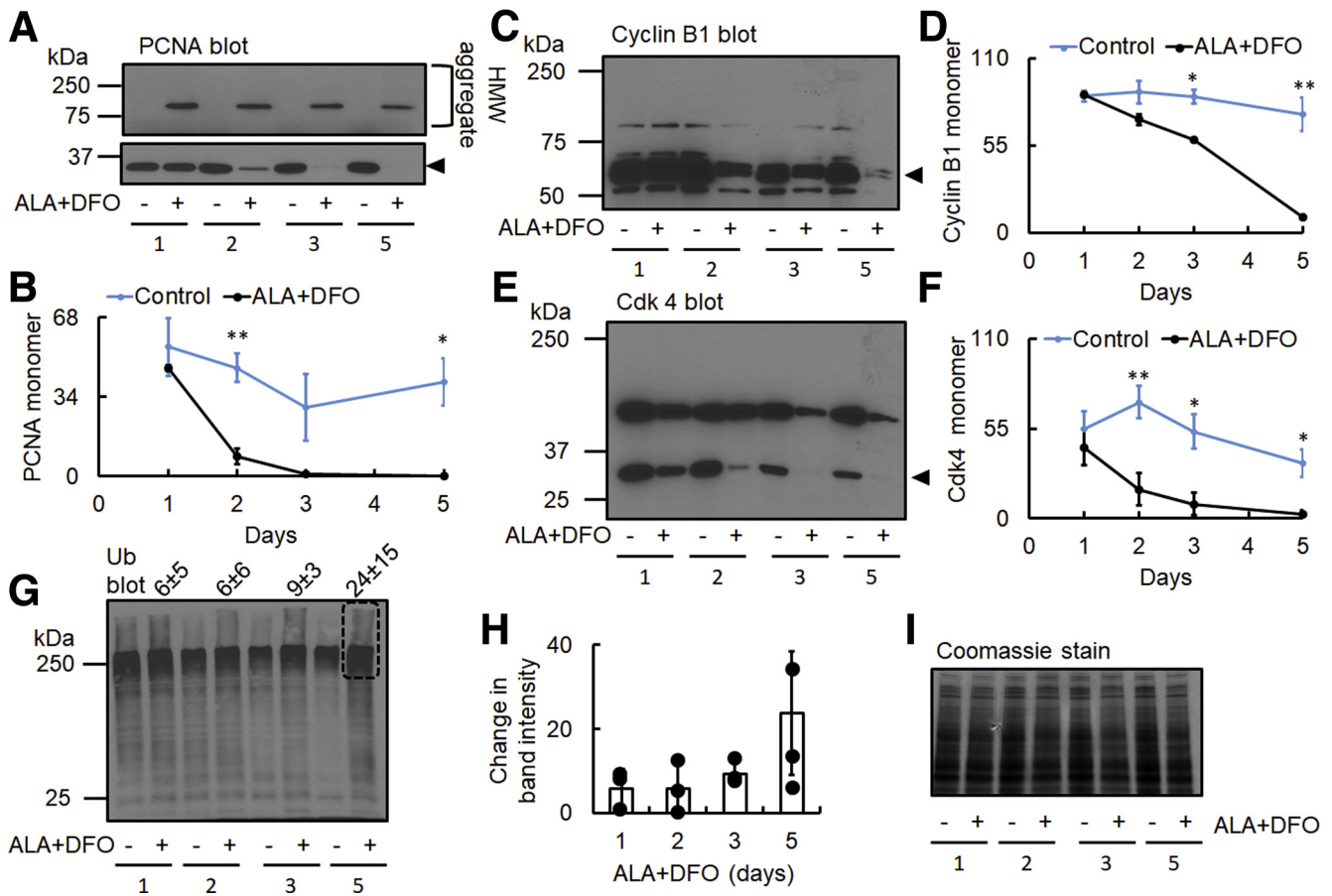


Figure 14. Aggregation of cell-cycle proteins occurs upon cell growth arrest in response to ALA + DFO treatment. Cell extracts from the experiment shown in Figure 13 were tested by blotting using antibodies to the indicated proteins (arrowhead denotes the monomer). The blots are representative of 3 independent experiments. (A) For the proliferating cell nuclear antigen (PCNA) blot, the monomer band was visualized after exposing the membrane for 5 seconds, and the HMW aggregate was visualized after overnight exposure. (B, D, and F) The band intensities are expressed as the average of 3 independent experiments with error bars representing the standard error of measurement. Statistical significance was determined using an unpaired *t* test (2-tailed). **P* < .05, ***P* < .008 and denotes comparison with control. (G) For the ubiquitin (Ub) blot, the difference in band intensity (between control and ALA + DFO-treated samples) of the region highlighted by the dotted box was used to quantify the extent of Ub protein accumulation. The mean change in band intensity \pm SD (N = 3) also is included at the top of the Ub blot. (H) The average of 3 independent experiments with error bars representing SD. (I) Coomassie staining of a representative gel is included to show near-equal protein loading. The blots are representative of 3 independent experiments.

with cobalt(III)-PP-IX in phosphate buffer.⁶¹ These findings raise the possibility that porphyrin-mediated oxidation and subsequent change of heptad periodicity initiates the porphyrin-protein-aggregated structures. Porphyrins bind to proteins by several types of noncovalent interactions between the porphyrin moiety and the amino acid side chain. Some examples of such interactions are CH- π and XH- π interactions,^{62,63} H-bonding and hydrophobic interactions,⁶⁴ and noncanonical interactions such as CH-O, CH-N, and a small percentage involving sulfur atoms.⁶⁵ In addition to porphyrin-protein associations, porphyrin-porphyrin interactions also occur.⁶⁶ A combination of porphyrin-porphyrin and porphyrin-protein interactions are reported to form mesoscale fibers consisting of a continuous lattice of peptides held together by transinteracting porphyrin moieties.⁶⁷ Several studies had been

performed on porphyrin binding to small peptides with formation of supramolecular aggregates,⁵⁸⁻⁶⁰ but we analyzed proteins in a complex biologic milieu. Although the precise binding mode remains to be defined, protein oxidation plays an important role in the process. Comparison of the IF protein oxidation pattern also showed heterogeneity in terms of the number of oxidized residues (Figure 7B), with K8 and K18 having a significantly higher number of oxidized residues compared with lamins. A prior study⁶⁸ showed that oxidation of M46 in glyceraldehyde-3-phosphate dehydrogenase led to its aggregation. For lamins, we observed oxidation in the conserved M352 (lamin A/C) and M353 (lamin B1) with an MQQ motif. Thus, oxidation of a small number of key residues might be sufficient to induce protein conformational changes that leads to aggregate formation.

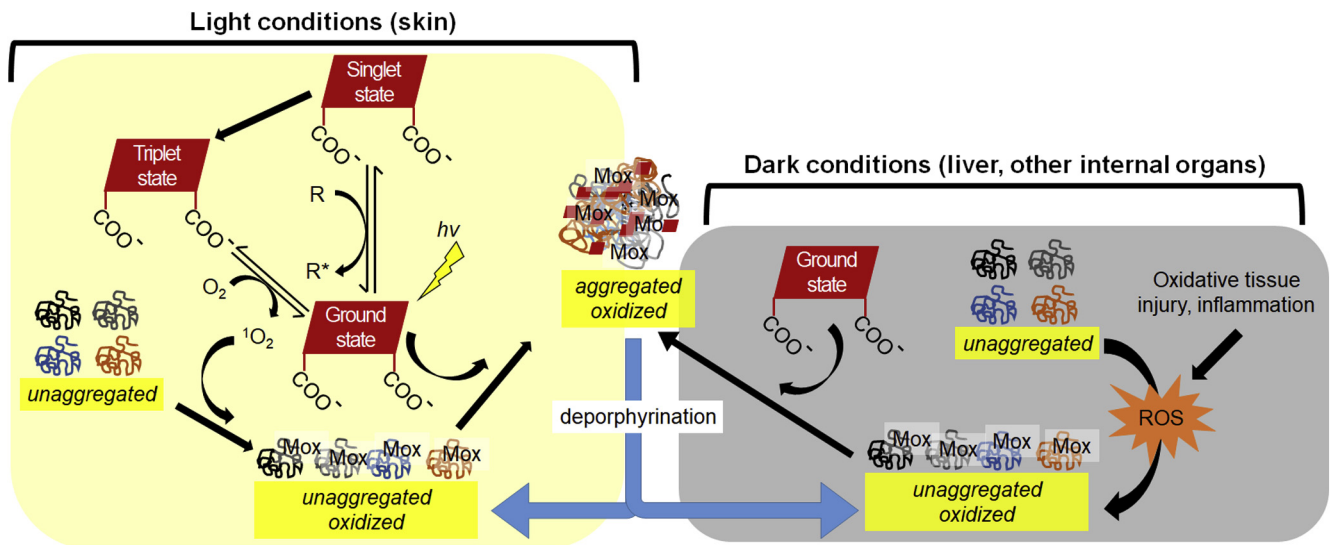


Figure 15. Schematic model of the mechanism of PP-IX-mediated protein aggregation. The schematic shows our proposed model of porphyrin-triggered protein aggregation in the presence and absence of light.

Porphyria as a Two-Hit Condition in Liver and Possibly Other Internal Organs

Our current and previous²³ work showed the unique ability of porphyrins to mediate protein aggregation in the presence of ambient light (Figure 15). However, porphyrin-induced damage is not limited to light-exposed tissues. For example, liver (a major source of porphyrin accumulation) also is damaged in hepatic porphyrias and in erythropoietic protoporphyria.^{3,4,6–15} Indeed, we observed, that in experimental models of porphyria such as DDC feeding, mouse livers accumulated protein aggregates.²³ Short-term DDC feeding (5 days) resulted in keratin aggregation and lamin B1 monomer loss, even in dark conditions.²³ This has been difficult to reconcile given the absence of photoactivation in internal organs. However, our findings indicate that porphyrins aggregate proteins independent of light if there is an additional oxidant source (Figure 11). Several contexts might promote light-independent generation of oxidative stress (Figure 15). For example, after DDC feeding there is an influx of inflammatory cells,^{69,70} with subsequent ROS generation including hypochlorous acid (from myeloperoxidase), O_2^- (from reduced nicotinamide adenine dinucleotide phosphate oxidase), and peroxynitrite (from nitric oxide synthase) that could provide the second oxidative hit and lead to protein oxidation and then formation of protein-porphyrin aggregates. In addition to inflammatory triggers, porphyrin accumulation might cause light-independent ROS by interacting with the hepatic cytochrome P450 system. For example, reduction of Uro to its anion radical by liver microsomal cytochrome P450 reductase, and subsequent formation of O_2^- , creates light-independent hepatic oxidative stress.^{71,72} Thus, for internal organs, porphyria in conjunction with oxidative stress from other parallel modes of injury jointly create the milieu for protein aggregation and proteotoxicity (reviewed by Maitra et al⁷³).

Porphyrin-Mediated Protein Aggregation Is a Disruptor of Cellular Homeostasis

Porphyrin accumulation and the ensuing protein aggregation have profound effects in altering cellular protein and organelle function, as exemplified by aggregation of ER stress-related proteins and activation of ER stress pathways.^{23,24} Similarly, porphyrin-mediated aggregation of nuclear lamins A/C and B1 is associated with significant nuclear shape distortion.²³ Another important component of cellular proteostasis is the proteasome, whereby porphyrin accumulation causes inhibition of proteasome peptidase activity.^{23,42,74} The function of the 19S subunit is to bind and then de-ubiquitinate ubiquitinated proteins, followed by directing them to the proteasome core for degradation.⁷⁵ Findings herein further show porphyrin-mediated aggregation of the 19S regulatory particle proteasome subunits, which likely contributes to the observed inhibition of proteasomal function. Thus, porphyrin-proteasome interaction impairs the proteasome through a 2-pronged mechanism: by inhibiting the peptidase activity,²³ and by impairing recognition of ubiquitinated substrates (Figure 12).

Another important cellular function that involves coordinated protein synthesis and degradation is cell-cycle progression. Previous studies have shown that treating cells with PP-IX for 12 hours caused cell-cycle arrest, but the mechanism of such arrest was not explored.⁷⁶ Our current data on ALA + DFO treatment of cells further highlights the role of porphyrin in disrupting normal cell-cycle progression via aggregation of important proteins involved in the process and blocking the cell cycle at all stages.

Conclusions

Porphyrins generate singlet oxygen via type II class reactions, which leads to protein oxidation and then aggregation through noncovalent porphyrin-protein interactions

(Figure 15). The deprotonation of the carboxylate moiety of PP-IX is essential for the ability of porphyrin to cause protein aggregation. Furthermore, PP-IX accumulation synergizes with other ROS to accentuate cell damage, which provides a potential mechanism for liver and other internal organ tissue injury that is independent of photoactivation. Collectively, these findings provide insight into the mechanism of tissue injury in porphyria, and might provide clues for designing improved photodynamic therapy strategies by harnessing the power of porphyrin's proteotoxicity.⁷⁷

Materials and Methods

Cell Lines and Mouse Husbandry

Huh7 cells (originally from the Japanese Collection of Research Bioresources Cell Bank) were a kind gift from Dr Lei Yin (University of Michigan). Huh7 cells were grown in Dulbecco's modified Eagle medium (Cellgro, Manassas, VA) supplemented with 10% fetal bovine serum (Sigma-Aldrich, St. Louis, MO). N/Tert keratinocytes were grown in K-SFM media (GIBCO/Invitrogen, Waltham, MA) supplemented with bovine pituitary extract (25 μ g/mL), epidermal growth factor (0.2 ng/mL), and 0.3 mmol/L CaCl₂ (all final concentrations). All animal studies were approved by the Animal Use and Care Committee at the University of Michigan. Male C57BL6 mice (age, 1 month) were fed 0.1% DDC (Sigma-Aldrich) followed by harvesting of livers.²³

Reagents

The reagents we used included the following: PP-IX, Zn-PP, TMPD, ethyl sorbate, sodium azide (NaN₃), mannitol, glucose oxidase, and superoxide dismutase were purchased from Sigma-Aldrich. Catalase was from Calbiochem (Burlington, MA). Hemin, Uro, and Copro were obtained from Frontier Scientific (Logan, UT). POBN was from Cayman Chemicals (Ann Arbor, MI). The following stock solutions were prepared for subsequent use: PP-IX (1.78 mmol/L in dimethylacetamide [DMA]); hemin (1.53 mmol/L in 100 mmol/L NaOH); Zn-PP (0.5 mmol/L in DMA); Uro (5 mmol/L in 100 mmol/L NaOH); Copro (5 mmol/L in 100 mmol/L NaOH); NaN₃ (100 mmol/L in 400 mmol/L phosphate buffer, pH 7.4); mannitol (100 mmol/L in 400 mmol/L phosphate buffer, pH 7.4); TMPD (121.7 mmol/L in DMA); and trolox (100 mmol/L in DMA). A detailed list of the reagents used is included in [Appendix I](#).

Porphyrin Treatment, SDS-PAGE, and Immunoblotting

Huh7 cells were lysed with 1% Nonidet P-40 (NP-40) in phosphate-buffered saline (PBS) (pH 7.4) containing 5 mmol/L EDTA and protease inhibitors cocktail (catalog 78410; ThermoScientific, Waltham MA) and spun at 14,000g for 10 minutes at 4°C. The insoluble pellet fraction was solubilized with 1% Empigen BB (in PBS, pH 7.4, containing 5 mmol/L EDTA and protease inhibitors cocktail; catalog 78410; ThermoScientific). The final composition of the reaction mixture was 0.5 mg/mL protein \pm 25 μ mol/L of the indicated porphyrin derivatives in 400 mmol/L phosphate buffer (pH

7.4). Control reactions comprised the same concentration of the solvent vehicle, either NaOH (for water-soluble porphyrin derivatives) or DMA. For pH titration experiments, the reaction mixture was prepared in 400 mmol/L NaH₂PO₄ (pH 4.5) or 400 mmol/L Na₂HPO₄ (pH 8.9). After incubating the reaction mixture (30 min, 37°C in light conditions), reducing Laemmli sample buffer was added and 10 μ g of protein was separated on SDS-PAGE and either stained with Coomassie blue (to visualize the proteins) or transferred to polyvinylidene fluoride membranes for immunoblotting. For visualization of immunoblots, horseradish-peroxidase-conjugated secondary antibody was used. After incubating the polyvinylidene fluoride membrane with secondary antibody the membrane was washed, then the chemiluminescence substrate was added, and the ensuing chemiluminescence was captured by exposing radiograph film to the polyvinylidene fluoride membrane. Different exposure times from the same membrane were captured to record low-intensity and high-intensity signals. The antibodies used included those directed to lamin A/C, ubiquitin (Santa Cruz Biotechnology, Inc, Dallas, TX), lamin B1, p62 (Abcam, Cambridge, MA), K5, K8 (clone TS1) and K18 (clone DC10), RPN5 (ThermoScientific), K8 (clone Troma 1) (Developmental Studies Hybridoma Bank, Iowa City, IA) and K18 (antibody 4468),⁷⁸ protein disulfide isomerase (Cell Signaling Technology, Danvers, MA), cyclin B1, and cyclin-dependent kinase 4 (Clontech, Mountain view, CA).

Western Blot Quantification

After developing the radiograph films, the films were scanned at 600-dots per inch resolution using a Cannon CanoScan LiDE 110 scanner (Cannon, Melville, NY). The band intensities from digitized images were quantified using ImageJ software (developed by National Institutes of Health, Bethesda, MD, and freely available at <https://imagej.nih.gov/ij/download.html>). The values shown are averages of 3 independent experiments \pm standard error of measurement.

Porphyrin Measurement

Cell or tissue lysates (2 μ L) were added to 200 μ L of a 1:1 mixture of ethanol:perchloric acid (0.9 N). The fluorescence was measured in a Biotek Synergy HT 96-well plate reader (Biotek, Winooski, VT) using the filter sets 400/30 nm (excitation) and 590/35 nm (emission). The amount of porphyrin in the experimental samples was calculated by comparing the fluorescence value with a standard curve prepared using a known concentration of porphyrins.

Continuous Wave EPR Spectral Analysis

Huh7 cell were lysed with Empigen buffer (as earlier), then adjusted to 4 mg/mL protein concentration and treated with PP-IX (200 μ mol/L, 15 min) in phosphate buffer (400 mmol/L, pH 7.4). The reaction mixture was supplemented with POBN as a spin trap (36 mmol/L final concentration). Where indicated, the reaction mixture also was supplemented with 20 mmol/L NaN₃. Spectra were collected at 22°C using a flat cell with the following experimental

conditions: microwave frequency, 9.7 GHz; modulation amplitude, 2 G; time constant, 1310.72 ms; scan time, 3335.544 s; and number of points, 1024.

Porphyryn Extraction

Huh7 cells were treated with 5 $\mu\text{mol/L}$ PP-IX in serum-free Dulbecco's modified Eagle medium (1 h), then lysed with 1% NP-40 in PBS (pH 7.4 with 5 mmol/L EDTA) supplemented with protease inhibitors. After lysis, the NP-40 insoluble fraction (pellet) was dissolved in RIPA buffer (25 mmol/L Tris-HCl, pH 7.6, 150 mmol/L NaCl, 1% NP-40, 1% sodium deoxycholate, 0.1% SDS, supplemented with protease inhibitor) and then sonicated using 10–15 one-second pulses (4°C). The RIPA-solubilized fraction was divided into 3 equal aliquots and used as follows: (1) as is, (2) to perform high salt extraction,⁷⁹ and (3) for acidified n-butanol extraction by mixing 100 μL of RIPA lysate with 850 μL of n-butanol and 50 μL of 0.1 N perchloric acid. The suspension then was pelleted (14,000 rpm, 4°C, 20 min). The supernatant was discarded and the pellet was washed once with -20°C chilled acetone and then suspended by sonicating in RIPA buffer followed by measuring the protein (BCA assay) and porphyrin levels.

For the tissue extractions, snap-frozen livers were collected from DDC-fed mice and then homogenized in a glass Dounce in 1% NP-40-containing buffer. The insoluble pellet fraction was processed in the same manner as described for Huh7 cells.

Protein Oxidation and Free Amino Acid Oxidation Analysis

Huh7 cells, grown in 150-mm dishes, were treated with PP-IX (5 $\mu\text{mol/L}$, 1 h), followed by collecting the cells by scraping, and then washing twice with PBS. The cell pellet then was suspended in 200 μL of deionized water, incubated for 20 minutes, 800 μL of methanol was added, mixed well, and then pelleted (4696g, 30 min, 4°C). The supernatant was collected and dried using a Speedvac vacuum concentrator (ThermoFisher Scientific, Waltham, MA) and then used for free amino acid oxidation analysis (methionine, met-sulfoxide, and met-sulfone) using liquid chromatography and MS. The pellet was resuspended by sonicating in Tris buffer (50 mmol/L, pH 8) containing 8 mol/L urea. After porphyrin and BCA assay measurement, the solutions were used for proteomic analysis as described.^{22,23} Aliquots also were examined by immune blotting.

Calculation for Fold Change in Protein Oxidation After PP-IX Treatment of Native Vs Predenatured Protein

The following equations were used:

$$\text{Fold change} = \frac{\left(\frac{A_{PP-IX}^{95C}}{T_{PP-IX}^{95C}}\right) - \left(\frac{A_{Control}^{95C}}{T_{Control}^{95C}}\right)}{\left(\frac{A_{PP-IX}}{T_{PP-IX}}\right) - \left(\frac{A_{Control}}{T_{Control}}\right)},$$

for 95°C denatured samples

$$\text{Fold change} = \frac{\left(\frac{A_{PP-IX}^{2\%SDS}}{T_{PP-IX}^{2\%SDS}}\right) - \left(\frac{A_{Control}^{2\%SDS}}{T_{Control}^{2\%SDS}}\right)}{\left(\frac{A_{PP-IX}}{T_{PP-IX}}\right) - \left(\frac{A_{Control}}{T_{Control}}\right)},$$

for 2% denatured samples

where, $A_{Control}$, A_{PP-IX} = abundance of peptides with oxidized residues in vehicle-treated ($A_{Control}$) and PP-IX-treated (A_{PP-IX}) samples, in nondenaturing conditions. $A_{Control}^{95C}$, A_{PP-IX}^{95C} = abundance of peptides with oxidized residues in vehicle-treated ($A_{Control}^{95C}$) and PP-IX-treated (A_{PP-IX}^{95C}) samples, predenatured by heating to 95°C for 3 minutes. $A_{Control}^{2\%SDS}$, $A_{PP-IX}^{2\%SDS}$ = same as described earlier, but samples were predenatured by 2% SDS. $T_{Control}$, T_{PP-IX} , $T_{Control}^{95C}$, T_{PP-IX}^{95C} , $T_{Control}^{2\%SDS}$, $T_{PP-IX}^{2\%SDS}$ = total peptide abundance.

Liquid Chromatography–Mass Spectrometric Analysis of PP-IX

Huh7 cells were lysed with 1% NP-40 in PBS (pH 7.4) containing 5 mmol/L EDTA and a protease inhibitor cocktail (catalog 78410; ThermoScientific), and then pelleted (14,000g, 10 min, 4°C). The pellet fraction was solubilized with 1% Empigen BB (in PBS, pH 7.4, containing 5 mmol/L EDTA and protease inhibitor cocktail). Protein content was quantified using a BCA assay (catalog 23225; ThermoScientific). The final composition of the reaction mixture was 1 mg/mL protein and 50 $\mu\text{mol/L}$ PP-IX in 400 mmol/L phosphate buffer (pH 7.4). Control reactions consisted of 50 $\mu\text{mol/L}$ PP-IX in 400 mmol/L phosphate buffer (pH 7.4). After incubating the samples for 30 minutes, at 22°C, under ambient lighting, PP-IX was extracted using 4 volumes of chilled methanol (-20°C), followed by pelleting (4696g, 20 min, 4°C). The supernatant was collected and analyzed by an Agilent Q-TOF (Santa Clara, CA) mass spectrometer equipped with an ultra-high-pressure liquid chromatography system with a binary pump, an autosampler with thermostatic temperature control, a photodiode array detector, and Agilent Masshunter Data Acquisition software. A reverse-phase octadecylsilica (C18) (Zorbax eclipse plus, 201 mm \times 50 mm dimension, 1.8- μm particle size, Agilent part 959757-902, Santa Clara, CA) column was used. The flow rate was 0.4 mL/min with linear gradients of solvents A and B (A, 0.1% formic acid in water; B, 0.1% formic acid in acetonitrile). The solvent gradient was as follows: 0–1 minute, 5% B; 1–8 minutes, 100% B; and 8–10 minutes, 100% B. The column was equilibrated with 95% solvent A for 2 minutes between every injection. Liquid chromatography electrospray ionization MS in the positive modes were performed using the following parameters: drying gas flow of 5 L/min, drying gas temperature of 325°C, and mass range between m/z 52 and m/z 3200 was scanned to obtain full scan mass spectra. Under these conditions, PP-IX ion was detected at $(M + H)^+$ 563. The photodiode array detector was set at 400 nm to obtain the chromatogram.

Fluorescence-Activated Cell Sorter Analysis for Cellular DNA Content

Huh7 cells (2.1×10^6) were plated on 150-mm tissue culture dishes. After 1 day, the media was switched to include ALA (1 mmol/L) and DFO (100 μ mol/L). The cells then were harvested by trypsinization at the indicated time points after initiating the ALA + DFO treatment. Cell viability was estimated using Trypan blue. For fluorescence-activated cell sorter analysis, 10^6 cells/sample were used. The cells were fixed with ethanol and stained with the nuclear stain FxCycle Far Red (ThermoFisher), and analyzed using a Bio-Rad (Hercules, CA) ZE5 cell analyzer.

Statistical Analysis

Statistical analysis of the immunoblot relative band intensities, porphyrin measurements, area under the curve of metabolites (from mass spectrometric experiments), cell viability using Trypan blue staining, and fluorescence-activated cell sorter analysis were performed using GraphPad Prism software (GraphPad Software, San Diego, CA). Statistical comparisons were performed using the unpaired *t* test (2-tailed).

References

- Schultz IJ, Chen C, Paw BH, Hamza I. Iron and porphyrin trafficking in heme biogenesis. *J Biol Chem* 2010; 285:26753–26759.
- Ajioka RS, Phillips JD, Kushner JP. Biosynthesis of heme in mammals. *Biochim Biophys Acta* 2006;1763:723–736.
- Balwani M, Desnick RJ. The porphyrias: advances in diagnosis and treatment. *Blood* 2012;120:4496–4504.
- Puy H, Gouya L, Deybach JC. Porphyrias. *Lancet* 2010; 375:924–937.
- Bonkovsky HL, Guo JT, Hou W, Li T, Narang T, Thapar M. Porphyrin and heme metabolism and the porphyrias. *Compr Physiol* 2013;3:365–401.
- Ramanujam VM, Anderson KE. Porphyria diagnostics-part 1: a brief overview of the porphyrias. *Curr Protoc Hum Genet* 2015;86, 17.20.1–6.
- Singal AK, Parker C, Bowden C, Thapar M, Liu L, McGuire BM. Liver transplantation in the management of porphyria. *Hepatology* 2014;60:1082–1089.
- Sardh E, Wahlin S, Bjornstedt M, Harper P, Andersson DE. High risk of primary liver cancer in a cohort of 179 patients with Acute Hepatic Porphyria. *J Inherit Metab Dis* 2013;36:1063–1071.
- Singal AK, Anderson KE. Variegated porphyria. In: Adam MP, Ardinger HH, Pagon RA, Wallace SE, Bean LJH, Stephens K, Amemiya A, eds. *GeneReviews*(R). Seattle, WA: 1993.
- Wang B, Bissell DM. Hereditary coproporphyrin. In: Adam MP, Ardinger HH, Pagon RA, Wallace SE, Bean LJH, Stephens K, Amemiya A, eds. *GeneReviews*(R). Seattle, WA: 1993.
- Liu LU, Phillips J, Bonkovsky H. Familial porphyria cutanea tarda. In: Adam MP, Ardinger HH, Pagon RA, Wallace SE, Bean LJH, Stephens K, Amemiya A, eds. *GeneReviews*(R). Seattle, WA: 1993.
- Erwin A, Balwani M, Desnick RJ. Congenital erythropoietic porphyria. In: Adam MP, Ardinger HH, Pagon RA, Wallace SE, Bean LJH, Stephens K, Amemiya A, eds. *GeneReviews*(R). Seattle, WA: 1993.
- Balwani M, Bloomer J, Desnick R. Erythropoietic protoporphyria, autosomal recessive. In: Adam MP, Ardinger HH, Pagon RA, Wallace SE, Bean LJH, Stephens K, Amemiya A, eds. *GeneReviews*(R). Seattle, WA: 1993.
- Balwani M, Bloomer J, Desnick R. X-linked protoporphyria. In: Adam MP, Ardinger HH, Pagon RA, Wallace SE, Bean LJH, Stephens K, Amemiya A, eds. *GeneReviews*(R). Seattle, WA: 1993.
- Whitley SD, Badminton MN. Acute intermittent porphyria. In: Adam MP, Ardinger HH, Pagon RA, Wallace SE, Bean LJH, Stephens K, Amemiya A, eds. *GeneReviews*(R). Seattle, WA: 1993.
- Foote CS. Definition of type I and type II photosensitized oxidation. *Photochem Photobiol* 1991;54:659.
- Casanova-Gonzalez MJ, Trapero-Marugan M, Jones EA, Moreno-Otero R. Liver disease and erythropoietic protoporphyria: a concise review. *World J Gastroenterol* 2010;16:4526–4531.
- Takeshita K, Takajo T, Hirata H, Ono M, Utsumi H. In vivo oxygen radical generation in the skin of the protoporphyria model mouse with visible light exposure: an L-band ESR study. *J Invest Dermatol* 2004;122:1463–1470.
- Brun A, Sandberg S. Mechanisms of photosensitivity in porphyric patients with special emphasis on erythropoietic protoporphyria. *J Photochem Photobiol B* 1991; 10:285–302.
- Schultz I. Ein Fall von Pemphigus leprosus, kompliziert durch Leprosia viscer. Inaug. Diss Greifswald 1874.
- With TK. A short history of porphyrins and the porphyrias. *Int J Biochem* 1980;11:189–200.
- Singla A, Griggs NW, Kwan R, Snider NT, Maitra D, Ernst SA, Herrmann H, Omary MB. Lamin aggregation is an early sensor of porphyria-induced liver injury. *J Cell Sci* 2013;126:3105–3112.
- Maitra D, Elenbaas JS, Whitesall SE, Basrur V, D'Alecy LG, Omary MB. Ambient light promotes selective subcellular proteotoxicity after endogenous and exogenous porphyrinogenic stress. *J Biol Chem* 2015;290:23711–23724.
- Elenbaas JS, Maitra D, Liu Y, Lentz SI, Nelson B, Hoenerhoff MJ, Shavit JA, Omary MB. A precursor-inducible zebrafish model of acute protoporphyria with hepatic protein aggregation and multiorganellar stress. *FASEB J* 2016;30:1798–1810.
- Knobler E, Poh-Fitzpatrick MB, Kravetz D, Vincent WR, Muller-Eberhard U, Vincent SH. Interaction of hemopexin, albumin and liver fatty acid-binding protein with protoporphyria. *Hepatology* 1989;10:995–997.
- Papadopoulos V, Baraldi M, Guilarte TR, Knudsen TB, Lacapere JJ, Lindemann P, Norenberg MD, Nutt D, Weizman A, Zhang MR, Gavish M. Translocator protein (18kDa): new nomenclature for the peripheral-type benzodiazepine receptor based on its structure and molecular function. *Trends Pharmacol Sci* 2006; 27:402–409.
- Ross CA, Poirier MA. Protein aggregation and neurodegenerative disease. *Nat Med* 2004;10(Suppl):S10–S17.
- Zatloukal K, French SW, Stumptner C, Strnad P, Harada M, Toivola DM, Cadrin M, Omary MB. From

- Mallory to Mallory-Denk bodies: what, how and why? *Exp Cell Res* 2007;313:2033–2049.
29. Tanielian C, Wolff C. Porphyrin-sensitized generation of singlet molecular oxygen: comparison of steady-state and time-resolved methods. *J Physical Chem* 1995; 99:9825–9830.
 30. Barbosa Neto NM, Correa DS, De Boni L, Parra GG, Misoguti L, Mendonça CR, Borissevitch IE, Zilio SC, Gonçalves PJ. Excited states absorption spectra of porphyrins – solvent effects. *Chem Physics Lett* 2013; 587:118–123.
 31. Genaro-Mattos TC, Queiroz RF, Cunha D, Appolinario PP, Di Mascio P, Nantes IL, Augusto O, Miyamoto S. Cytochrome c reacts with cholesterol hydroperoxides to produce lipid- and protein-derived radicals. *Biochemistry* 2015;54:2841–2850.
 32. Kubat P, Zelinger Z, Jirsa M. The effect of the irradiation wavelength on the processes sensitized by protoporphyrin IX dimethyl ester. *Radiat Res* 1997;148:382–385.
 33. Yee KK, Soo KC, Bay BH, Olivo M. A comparison of protoporphyrin IX and protoporphyrin IX dimethyl ester as a photosensitizer in poorly differentiated human nasopharyngeal carcinoma cells. *Photochem Photobiol* 2002;76:678–682.
 34. Dickson MA, Hahn WC, Ino Y, Ronfard V, Wu JY, Weinberg RA, Louis DN, Li FP, Rheinwald JG. Human keratinocytes that express hTERT and also bypass a p16(INK4a)-enforced mechanism that limits life span become immortal yet retain normal growth and differentiation characteristics. *Mol Cell Biol* 2000;20:1436–1447.
 35. Rheinwald JG, Hahn WC, Ramsey MR, Wu JY, Guo Z, Tsao H, De Luca M, Catricala C, O'Toole KM. A two-stage, p16(INK4A)- and p53-dependent keratinocyte senescence mechanism that limits replicative potential independent of telomere status. *Mol Cell Biol* 2002;22:5157–5172.
 36. Davies MJ. Reactive species formed on proteins exposed to singlet oxygen. *Photochem Photobiol Sci* 2004;3:17–25.
 37. Ehrenshaft M, Zhao B, Andley UP, Mason RP, Roberts JE. Immunological detection of N-formylkynurenine in porphyrin-mediated photooxidized lens alpha-crystallin. *Photochem Photobiol* 2011;87:1321–1329.
 38. Herrmann H, Aebi U. Intermediate filaments: molecular structure, assembly mechanism, and integration into functionally distinct intracellular Scaffolds. *Annu Rev Biochem* 2004;73:749–789.
 39. Krieg M, Whitten DG. Self-sensitized photooxidation of protoporphyrin IX and related free-base porphyrins in natural and model membrane systems. Evidence for novel photooxidation pathways involving amino acids. *J Am Chem Soc* 1984;106:2477–2479.
 40. Cox GS, Krieg M, Whitten DG. Photochemical reactivity in organized assemblies. 30. Self-sensitized photooxidation of protoporphyrin IX derivatives in aqueous surfactant solutions; product and mechanistic studies. *J Am Chem Soc* 1982;104:6930–6937.
 41. Krieg M, Whitten DG. Self-sensitized photo-oxidation of protoporphyrin IX and related porphyrins in erythrocyte ghosts and microemulsions: a novel photo-oxidation pathway involving singlet oxygen. *J Photochem* 1984; 25:235–252.
 42. Singla A, Moons DS, Snider NT, Wagenmaker ER, Jayasundera VB, Omary MB. Oxidative stress, Nrf2 and keratin up-regulation associate with Mallory-Denk body formation in mouse erythropoietic protoporphyria. *Hepatology* 2012;56:322–331.
 43. Kelman Z. PCNA: structure, functions and interactions. *Oncogene* 1997;14:629–640.
 44. Strauss B, Harrison A, Coelho PA, Yata K, Zernicka-Goetz M, Pines J. Cyclin B1 is essential for mitosis in mouse embryos, and its nuclear export sets the time for mitosis. *J Cell Biol* 2018;217:179–193.
 45. Du Z, Tong X, Ye X. Cyclin D1 promotes cell cycle progression through enhancing NDR1/2 kinase activity independent of cyclin-dependent kinase 4. *J Biol Chem* 2013;288:26678–26687.
 46. Harada M, Hanada S, Toivola DM, Ghori N, Omary MB. Autophagy activation by rapamycin eliminates mouse Mallory-Denk bodies and blocks their proteasome inhibitor-mediated formation. *Hepatology* 2008; 47:2026–2035.
 47. Langendonk JG, Balwani M, Anderson KE, Bonkovsky HL, Anstey AV, Bissell DM, Bloomer J, Edwards C, Neumann NJ, Parker C, Phillips JD, Lim HW, Hamzavi I, Deybach JC, Kauppinen R, Rhodes LE, Frank J, Murphy GM, FPJ Karstens, Sijbrands EJG, de Rooij FWM, Lebowitz M, Naik H, Goding CR, Wilson JHP, Desnick RJ. Afamelanotide for erythropoietic protoporphyria. *N Engl J Med* 2015; 373:48–59.
 48. Porter RM, Anstey A. Evidence and conjecture about mechanisms of cutaneous disease in photodermatology. *Exp Dermatol* 2014;23:543–546.
 49. Minder EI, Schneider-Yin X, Steurer J, Bachmann LM. A systematic review of treatment options for dermal photosensitivity in erythropoietic protoporphyria. *Cell Mol Biol (Noisy-le-grand)* 2009;55:84–97.
 50. Moan J, Berg K. The photodegradation of porphyrins in cells can be used to estimate the lifetime of singlet oxygen. *Photochem Photobiol* 1991;53:549–553.
 51. Pattison DI, Rahmanto AS, Davies MJ. Photo-oxidation of proteins. *Photochem Photobiol Sci* 2012;11:38–53.
 52. Klaper M, Fudickar W, Linker T. Role of distance in singlet oxygen applications: a model system. *J Am Chem Soc* 2016;138:7024–7029.
 53. Zheng L, Nukuna B, Brennan ML, Sun M, Goormastic M, Settle M, Schmitt D, Fu X, Thomson L, Fox PL, Ischiropoulos H, Smith JD, Kinter M, Hazen SL. Apolipoprotein A-I is a selective target for myeloperoxidase-catalyzed oxidation and functional impairment in subjects with cardiovascular disease. *J Clin Invest* 2004;114:529–541.
 54. Parry DA, Steinert PM. Intermediate filaments: molecular architecture, assembly, dynamics and polymorphism. *Q Rev Biophys* 1999;32:99–187.
 55. Banerjee S, Wu Q, Ying Y, Li Y, Shirota M, Neculai D, Li C. In silico predicted structural and functional insights of all missense mutations on 2B domain of K1/K10 causing genodermatoses. *Oncotarget* 2016;7:52766–52780.
 56. Lee CH, Kim MS, Chung BM, Leahy DJ, Coulombe PA. Structural basis for heteromeric assembly and

- perinuclear organization of keratin filaments. *Nat Struct Mol Biol* 2012;19:707–715.
57. Strnad P, Zatloukal K, Stumptner C, Kulaksiz H, Denk H. Mallory-Denk-bodies: lessons from keratin-containing hepatic inclusion bodies. *Biochim Biophys Acta* 2008;1782:764–774.
 58. Apostolovic B, Danial M, Klok HA. Coiled coils: attractive protein folding motifs for the fabrication of self-assembled, responsive and bioactive materials. *Chem Soc Rev* 2010;39:3541–3575.
 59. Biscaglia F, Frezza E, Zurlo E, Gobbo M. Linker dependent chirality of solvent induced self-assembled structures of porphyrin-alpha-helical peptide conjugates. *Org Biomol Chem* 2016;14:9568–9577.
 60. Dosselli R, Ruiz-Gonzalez R, Moret F, Agnolon V, Compagnin C, Mognato M, Sella V, Agut M, Nonell S, Gobbo M, Reddi E. Synthesis, spectroscopic, and photophysical characterization and photosensitizing activity toward prokaryotic and eukaryotic cells of porphyrin-magainin and -buforin conjugates. *J Med Chem* 2014;57:1403–1415.
 61. Zaytsev DV, Xie F, Mukherjee M, Bludin A, Demeler B, Breece RM, Tierney DL, Ogawa MY. Nanometer to millimeter scale peptide-porphyrin materials. *Biomacromolecules* 2010;11:2602–2609.
 62. Medakovic VB, Milcic MK, Bogdanovic GA, Zaric SD. C-H...pi interactions in the metal-porphyrin complexes with chelate ring as the H acceptor. *J Inorg Biochem* 2004;98:1867–1873.
 63. Stojanovic SD, Medakovic VB, Predovic G, Beljanski M, Zaric SD. XH/pi interactions with the pi system of porphyrin ring in porphyrin-containing proteins. *J Biol Inorg Chem* 2007;12:1063–1071.
 64. Stojanovic SD, Zaric SD. Hydrogen bonds and hydrophobic interactions of porphyrins in porphyrin-containing proteins. *Open Structural Biol J* 2009;3:34–41.
 65. Stojanovic S, Isenovic ER, Zaric BL. Non-canonical interactions of porphyrins in porphyrin-containing proteins. *Amino Acids* 2012;43:1535–1546.
 66. Scolaro LM, Castriciano M, Romeo A, Patanè S, Cefalì E, Allegrini M. Aggregation behavior of protoporphyrin IX in aqueous solutions: clear evidence of vesicle formation. *J Physical Chem B* 2002;106:2453–2459.
 67. Pepe-Mooney BJ, Kokona B, Fairman R. Characterization of mesoscale coiled-coil peptide-porphyrin complexes. *Biomacromolecules* 2011;12:4196–4203.
 68. Samson AL, Knaupp AS, Kass I, Kleinfeld O, Marijanovic EM, Hughes VA, Lupton CJ, Buckle AM, Bottomley SP, Medcalf RL. Oxidation of an exposed methionine instigates the aggregation of glyceraldehyde-3-phosphate dehydrogenase. *J Biol Chem* 2014;289:26922–26936.
 69. Fickert P, Stoger U, Fuchsbichler A, Moustafa T, Marschall HU, Weiglein AH, Tsybrovskyy O, Jaeschke H, Zatloukal K, Denk H, Trauner M. A new xenobiotic-induced mouse model of sclerosing cholangitis and biliary fibrosis. *Am J Pathol* 2007;171:525–536.
 70. Jemail L, Miyao M, Kotani H, Kawai C, Minami H, Abiru H, Tamaki K. Pivotal roles of Kupffer cells in the progression and regression of DDC-induced chronic cholangiopathy. *Sci Rep* 2018;8:6415.
 71. Morehouse KM, Moreno SN, Mason RP. The one-electron reduction of uroporphyrin I by rat hepatic microsomes. *Arch Biochem Biophys* 1987;257:276–284.
 72. Morehouse KM, Mason RP. The enzymatic one-electron reduction of porphyrins to their anion free radicals. *Arch Biochem Biophys* 1990;283:306–310.
 73. Maitra D, Bragazzi Cunha J, Elenbaas JS, Shavit JA, Omary MB. Porphyrin-induced protein oxidation and aggregation as a mechanism of porphyria associated cell injury. *Cell Mol Gastroenterol Hepatol* 2019. <https://doi.org/10.1016/j.jcmgh.2019.06.006>.
 74. Santoro AM, Lo Giudice MC, D'Urso A, Lauceri R, Purrello R, Milardi D. Cationic porphyrins are reversible proteasome inhibitors. *J Am Chem Soc* 2012;134:10451–10457.
 75. Livneh I, Cohen-Kaplan V, Cohen-Rosenzweig C, Avni N, Ciechanover A. The life cycle of the 26S proteasome: from birth, through regulation and function, and onto its death. *Cell Res* 2016;26:869–885.
 76. Li Q, Wang X, Zhang K, Li X, Liu Q, Wang P. DNA damage and cell cycle arrest induced by protoporphyrin IX in sarcoma 180 cells. *Cell Physiol Biochem* 2013;32:778–788.
 77. Zhang H, Ramakrishnan SK, Triner D, Centofanti B, Maitra D, Gyorffy B, Sebolt-Leopold JS, Dame MK, Varani J, Brenner DE, Fearon ER, Omary MB, Shah YM. Tumor-selective proteotoxicity of verteporfin inhibits colon cancer progression independently of YAP1. *Sci Signal* 2015;8:ra98.
 78. Tao GZ, Rott LS, Lowe AW, Omary MB. Hyposmotic stress induces cell growth arrest via proteasome activation and cyclin/cyclin-dependent kinase degradation. *J Biol Chem* 2002;277:19295–19303.
 79. Ku NO, Toivola DM, Zhou Q, Tao GZ, Zhong B, Omary MB. Studying simple epithelial keratins in cells and tissues. *Methods Cell Biol* 2004;78:489–517.

Received April 9, 2019. Accepted May 28, 2019.

Correspondence

Address correspondence to: Dhiman Maitra, PhD, Department of Molecular and Integrative Physiology, University of Michigan Medical School, 7720 Medical Science Building II, 1137 Catherine Street, Ann Arbor, Michigan 48109-5622. e-mail: dm1401@cabm.rutgers.edu; fax: (734) 936-8813.

Acknowledgments

The current address for Dhiman Maitra and M. Bishr Omary is Center for Advanced Biotechnology & Medicine, Rutgers University, Piscataway, New Jersey.

Author contributions

Dhiman Maitra, Eric L. Carter, Stephen W. Ragsdale, Nicolai Lehnert, and M. Bishr Omary conceptualized and designed the study; Dhiman Maitra, Eric L. Carter, Rani Richardson, Matthew W. Wolf, and Venkatesha Basrur acquired data; Dhiman Maitra, Eric L. Carter, Laure Rittié, Venkatesha Basrur, Alexey I. Nesvizhskii, Stephen W. Ragsdale, Nicolai Lehnert, and M. Bishr Omary analyzed and interpreted the data; Dhiman Maitra and M. Bishr Omary drafted the manuscript; Dhiman Maitra, Eric L. Carter, Rani Richardson, Laure Rittié, Venkatesha Basrur, Haoming Zhang, Alexey I. Nesvizhskii, Yoichi Osawa, Matthew W. Wolf, Stephen W. Ragsdale, Nicolai Lehnert, Harald Herrmann, and M. Bishr Omary critically revised the manuscript and provided important intellectual input; Haoming Zhang, Yoichi Osawa, Laure Rittié, and Harald Herrmann provided technical or material support; and M. Bishr Omary supervised the study. All authors had full access to the study data and reviewed and approved the final manuscript.

Conflicts of interest

The authors disclose no conflicts.

Funding

This work was supported by National Institutes of Health grant R01 DK116548 (M.B.O.), R01-GM123513 (SWR) and by National Institutes of Health award DK034933 to the University of Michigan. Also supported by a Summer Undergraduate fellowship (National Institutes of Health R25 DK096968) from the American Gastroenterological Association (R.R.).

Appendix I. Antibodies, Porphyrin Derivatives, and Cell Lines

Antibodies					
Name	Clone	Clonality	Vendor	Catalog no.	Lot no.
Lamin A/C	E-1	Monoclonal	Santa Cruz Biotechnology	sc-376248	
Ubiquitin	P4D1			sc-8017	
Lamin B1		Polyclonal	Abcam	ab16048	GR3214420-1
p62	EPR4844			ab109012	GR124843-73
PDI	C81H6	Monoclonal	Cell Signaling Technology	3501S	
PCNA	D3H8P			13110S	
K5	XM26	Monoclonal	ThermoFisherScientific	MA5-12596	
K8	TS-1			MA5-14428	
K18	DC-10			MA5-12104	
RPN1		Polyclonal		PA1-964	TD264496
K8	Troma I	Monoclonal	DSHB (Iowa City, IA)	TROMA-I	
K18	4468	Polyclonal	Antibody was generated against an N-terminal K18 peptide (26RPVSSAASVYAGA38) as described ⁷⁸		
Cyclin B1		Polyclonal	Clontech	S1185	7060364
Cdk4				S1193	7070438
Porphyryn derivatives					
PP-IX			Sigma-Aldrich	P8293	
Zn-PP				282820	
Hemin			Frontier Scientific (Logan, UT)	H651-9	
PP-Dim				P590-9	
Deu-PP				D510-9	
Uro				C654-3	
Copro				U830-3	
Cell lines					
Source					
Human n-TERT keratinocytes			Developed by Dr Jim Rheinwald ^{34,35} (Department of Dermatology, Brigham and Women's Hospital and Harvard Skin Disease Research Center) and provided by Dr Laure Rittié		
Huh7			Originally from the Japanese Collection of Research Bioresources Cell Bank; was a kind gift from Dr Lei Yin (University of Michigan)		

Deu-PP, deuteroporphyrin-IX; PCNA, proliferating cell nuclear antigen; PDI, protein disulfide isomerase.